Enhanced Fields of View in Epoxide Waveguide Arrays doped with Au Nanoparticles

Enhanced Fields of View in Epoxide Waveguide Arrays doped with Au Nanoparticles

By

Yi Pan, B.Sc. (Hons.)

A Thesis

Submitted to the School of Graduate Studies in Partial Fulfillment of the

Requirements for the Degree

Master of Science in Chemistry

McMaster University

MASTER OF SCIENCE (2018) **MCMASTER UNIVERSITY**

(Chemistry) Hamilton, Ontario

TITLE: Enhanced Fields of View in Epoxide Waveguide Arrays doped with Au nanoparticles

AUTHOR: Yi Pan, B.Sc. (Hons.)(University of Waterloo, Waterloo, Ontario, Canada)

SUPERVISOR: Dr. Kalaichelvi Saravanamuttu; Dr. Cecile Fradin

NUMBER OF PAGES: xiv, 70

Abstract

Polymer matrices doped with a dispersion of noble metal nanoparticles combine the strong plasmon resonance-based optical signatures of the latter with the flexibility and processability of the former. We have developed a nonlinear lithographic technique to generate large populations of epoxide waveguides containing a uniform dispersion of Au nanoparticles. The method is based on the self-trapping of multiple beams of white light propagating through a catonic polymerizable matrix doped with a gold salt, initiating the polymerization of epoxide moieties and simultaneously the *in situ* synthesis of elemental Au nanoparticles. Each white light filament inscribes a cylindrical waveguide, leading to an array of metallodielectric waveguides. Field of view (FOV) measurements indicate that the metallodielectric waveguide array has a nearly 59 % increase in FOV relative to its all-dielectric counterparts and can be tuned through the concentration of Au nanoparticles and the optical intensities employed to generate waveguides.

Acknowledgement

I would like to express my sincere gratitude to my supervisor, Dr. Kalaichelvi Saravanamuttu for providing me the precious opportunity to work as a graduate student in her group, for her invaluable insights, guidance and encouragement. I also would like to thank my co-supervisor, Dr. Cecile Fradin for her valuable inputs, encouragement and constructive suggestion.

I would like to thank my committee member, Dr. Ayse Turak for her positive feedbacks and great support.

I'm truly grateful to have the opportunity to work with such a great group of people in the lab. Many thanks to the past and present group members of Dr. Saravanamuttu, Alex Hudson, Derek Morim, Hao Lin, Oscar Herrera Cortes, Derek Morim, Kathryn Benincasa, Fariha Mahmood, Shaochang Song, Kyle Kavaseri, Thomas Pena Ventura, Heather Bolton, Wanchi Chang and Dinesh Kumar Basker for their valuable discussion, timely support and all the good time brought by them. Great thanks to Hao Lin and Dinesh Kumar Basker, who have shown that photoinduced *in situ* synthesis of gold-epoxide nanocomposite and the creation of compound eye mimic structure with large field of view based on polymer waveguides, from where I could easily initiate my research project. Special thanks to Hao Lin, who put a lot of inputs to help me establish my project, for all his critical thinking, support and encouragement.

Finally, I would greatly my parents, Chunying Wang and Qing Pan for their continuous support, love and encouragement.

Contents

List of Figures

List of Abbreviations

WG	Waveguide
FOV	Field of view
Δn	Change of the refractive index
k	Angular wavenumber
ψ	Electric field amplitude
WEL	Waveguide encoded lattice
RDWEL	Radially distributed waveguide encoded lattice
SPR	Surface plasmon resonance
MCVD	Modified chemical vapor deposition
NP	Nanoparticle
MI	Modulation instability
ERL-4221	3, 4-epoxycyclohexylmethyl-3', 4'-epoxycyclohexane carboxylate
pTHF	poly (1, 4-butanediol (M_n 250))
DMS	Epoxypropoxypropyl terminated polydimethylsiloxane

PS	Photosensitizer
PI	Photoinitiator
QTH	quartz tungsten halogen lamp
CCD	Charged-coupled device
TEM	Transmission electron microscopy
EDS	Energy dispersive X-ray spectroscopy
UV-vis	Ultraviolet–visible
FWHM	Full width at half maximum
EQE	External quantum efficiency

1 Introduction

The practical potential of hybrid materials is becoming more and more prominent due to their versatile and unique properties. Particularly, incorporating metal nanoparticles in polymers[1-6] becomes significant for functional devices used in spectroscopy, optical sensor[7] and optoelectronics. As a typical hybrid material, polymer matrices doped with a dispersion of noble metal nanoparticles are very promising, since they combine the strong plasmon resonance-based optical signatures of the latter with the flexibility and processibility of the former.[8]

1.1Bio-inspired waveguides (WGs) arrays

1.1.1 Compound eye-mimic structures based on waveguides

1.1.1.1 Natural and artificial compound eyes

As a visual organ of arthropods, natural compound eye consists of numerous ommatidia, which are independent photoreception units pointing to slightly different directions.[9] Each ommatidia contributes its own inputs to form the perceived image of the arthropod. Comparing to the single-aperture eyes, compound eyes with small volume possess large field of view (FOV), high sensitivity to motion and the ability to distinguish polarized light.[10]

For the artificial compound eyes, ommatidia essentially are waveguides. **Figure 1.1a** shows the artificial compound eye which containing numerous artificial ommatidium. **Figure 1.1b** is the scheme of artificial ommatidium which is composed of microlens, polymer cone, waveguide core, waveguide cladding and photodetector.

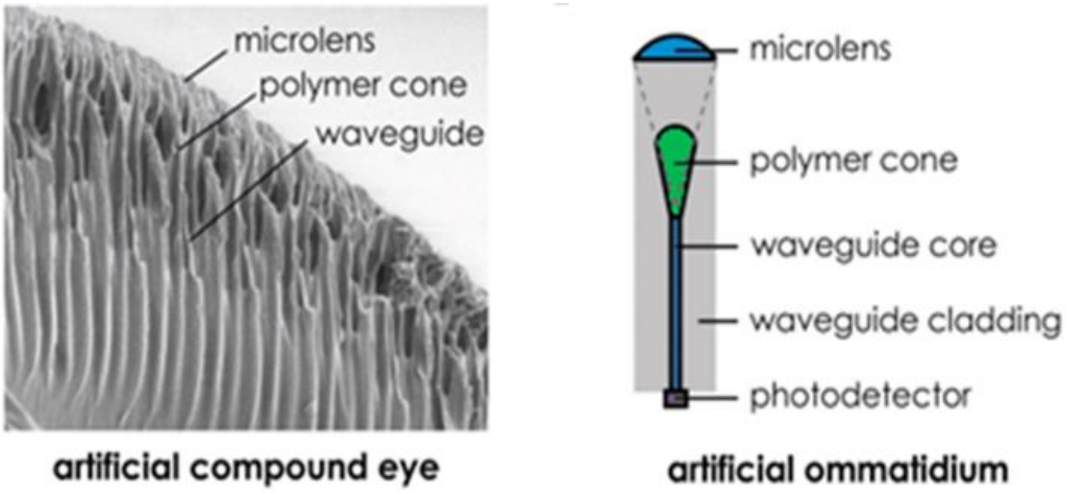

Figure 1.1 (a) The scheme of artificial compound eye. The scheme of artificial ommatidium. Reprinted with permission from the American Association for the Advancement of Science [11].

Compared with the single chamber optical system, the artificial compound eye has a lot of advantages. Since it is a single sensor with multiple waveguides and its captured image is the combination of the sub-image collected from each waveguide, which leads to a large FOV and achieves in sub-imaging processing. **Figure 1.2** is an example of the artificial compound eyes which gives a panoramic FOV.

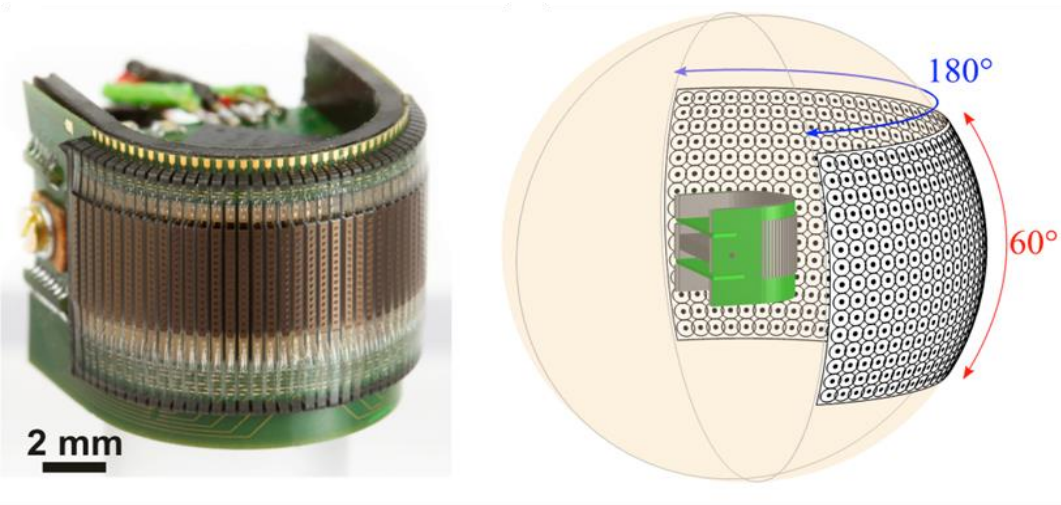

Figure 1.2 An example of the artificial compound eyes which gives a panoramic FOV. Reprinted with permission from Science. Reprinted with permission from National Academy of Science of the United States of American [12].

1.1.1.2 Compound eye-mimic artificial structures created in polymer matrix

Previous work of our group has shown that compound eye-mimic artificial structures can be created in polymer matrix. As well, we have developed a nonlinear lithographic technique to generate large populations of epoxide waveguides. When light propagating through a polymerizable matrix, it can initiate the photopolymerization, which lead to an increase in the localize density and a corresponding change of the refractive index. The change of refractive index will lead light to be self-focused. However, the balance between the self-focusing and natural divergence of light will lead it to be self-trapped. In this thesis work, a photomask (PhotomaskPORTAL, square grid pattern, periodicity = 40 μm) was used to split the uniform broad beam into individual narrow self-trapped filaments. Then, each self-trapped beam will inscribe a permanent cylindrical structure along

its propagation path which is waveguide. Therefore, the waveguides are self-induced during the irreversible photoinitiated polymerization.

Comparing the compound eye-mimic artificial structures created in polymer matrix to other types of artificial compound eyes, it has many advantages. It's cost effective, it can be fabricated just by using several optical assemblies and cheap polymerizable sol. However, most of the other types of artificial compound eyes use the multiple camera systems which requiring multiple lenses and multiple detector arrays.[13] As well, the fabrication process of compound eye-mimic artificial structures created in polymer matrix is very quick, can be done by a single step. As well, the compound eye-mimic artificial structures created in polymer matrix has outstanding FOV, which are illustrated in **Section 1.1.3.3** in this thesis.

1.1.2 Fabrication of polymerizable waveguide using nonlinear lithographic technique

1.1.2.1 Self-trapping of optical beams

When a single narrow optical beam propagating in a linear medium, it has natural tendency to diverge due to the diffraction and dispersion. However, when the beam propagating in nonlinear medium, i.e. photoresponsive material, the propagation results in an increase in refractive index. Then, the change of the refractive index (Δn) can lead the light to be self-focused. As a result, the balance between the divergence and self-focusing causes the initial divergent beam to be self-trapped.[14]

The following scheme shows the spatial beam profiles of a propagating beam when it undergoes natural diffraction, self-focusing and self-trapping.

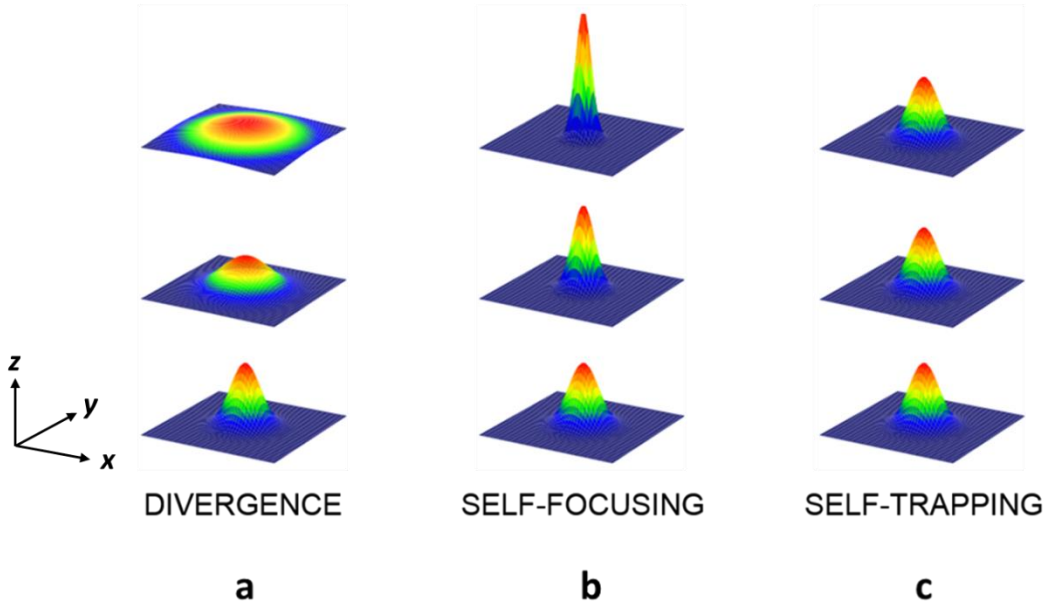

Figure 1.3 Scheme of the spatial beam profiles of a propagating beam when it undergoes (a) natural diffraction, (b) self-focusing and (c) self-trapping, where the color scale corresponds to intensity. From bottom to top, each column represents the spatial beam profile at different position along the direction of propagation. Reprinted with permission from [15].

1.1.2.2 The nonlinear Schrödinger equation

As mentioned above, the self-trapping of a beam is due to the counterbalance between its self-focusing and it natural divergence. During the propagation of a self-trapped beam, the spatial intensity profile of the beam stays unchanged and the resulting propagation path can be very long (much longer than Rayleigh length). When the divergence of a beam is exactly counterbalanced by its self-focusing, the

resulting self-trapped beam is defined as a soliton. The expression of the counterbalance can be explained by the nonlinear Schrödinger equation[14] as below:

$$2ik_0n_0\left(\frac{\partial\psi}{\partial z}\right) + \nabla_\perp^2\psi + k^2(n^2 - n_0^2)\psi = 0 \qquad \textbf{1-1}$$

For the **Equation 1-1**, k is the angular wavenumber and ψ stands for the electric field amplitude. Beam divergence can be expressed by the Laplacian term[14]:

$$\nabla_\perp^2 = \left({}^{\partial^2}/_{\partial x^2}\right) + \left({}^{\partial^2}/_{\partial y^2}\right) \qquad \textbf{1-2}$$

, where the plane of divergence is transverse to the propagation axis (i.e. axis z).

1.1.2.3 Self-trapping of coherent and incoherent light

For coherent beams, their amplitude and phase are completely time and space correlated. Whereas, the amplitude and phase of incoherent beams vary in time or in space, which have bad correlation. It is well known that laser is a common coherent light source while white light belongs to incoherent light sources. Plentiful researches on optical solitons have been theoretically and experimentally done with coherent light in the past 40 years. It was hard to generate solitons using incoherent sources due to their high uncorrelated nature.

However, the self-trapping of incoherent light is attracting more and more attentions recently. As an incoherent beam, white light contains many random bright-dark speckles whose fluctuations are at femtosecond timescale.[16] Some instantaneous media or conventional nonlinear media[17,18,19], such as Kerr media,

can response to the speckles at same timescale and lead the diverged white light beam to start self-focusing. As a result, femtosecond multiple filamentation of beam are obtained, which then randomly inscribe transient intersecting waveguides. To generate incoherent solitons, there are several critical conditions.[20-21] Firstly, incoherent solitons as a kind of solitons should be self-consisted, which means that the photoinduced waveguide can also guide the beam itself. Secondly, the response time of the nonlinear medium must be longer than the average time of fluctuation of the incoherent light. In this way, the medium would not response to the random speckles. Thirdly, in the nonlinear medium, the multimodal beam is supposed to induce multimodal waveguide in order to keep self-consistency of the entire optical field.

1.1.2.4 Self-trapping of white light in photopolymerizable matrix

Self-trapping of white light is facing a lot of challenges, since it contains many instantaneous speckles fluctuating rapidly and the multimodal beam. Due to the random bright-dark speckles fluctuating at femtosecond timescale, it's important to prevent the diffraction of the speckled beam from interfering self-trapping of white light. This requires the medium to have longer response time than the fluctuation time of the speckles. Thus, photopolymerizable medium as non-instantaneous medium, which have inherent longer response time, is ideal to elicit self-trapping of white light.[22-23]

As mentioned above, photopolymerizable media can overcome the limitations of other common medium, since they possess inherent non-instantaneous nonlinearity which help soliton propagation according to the change of refractive index. Polymerization as an irreversible chemical reaction in polymerizable medium can result in the nonlinear response to change the refractive index. During free radical polymerization, the increasing local density results in an increase in the refractive index, which consequently results in self-trapping of the white light.[24-26] Kewitsch et al. has demonstrated the following expression showing the temporal and spatial variation of refractive index change due to the free radical polymerization.[25]

$$\Delta n(x, y, z, t) = \Delta n_s \left\{1 - exp\left[-\frac{1}{U_0}\int_0^{t-\tau}|E(t)|^2 dt\right]\right\} \qquad \textbf{1-3}$$

where Δn_s represents the saturated refractive index change, τ is the lifetime of monomer radical, t is time, E(t) is the amplitude of the electric field and U_0 is the minimum energy required to initiate polymerization.

Our group has done several studies on self-trapping of incoherent light source. The studies showed the experimentally possibility of the nonlinear propagation of white light through photopolymerizable organosiloxane system.[27-30]

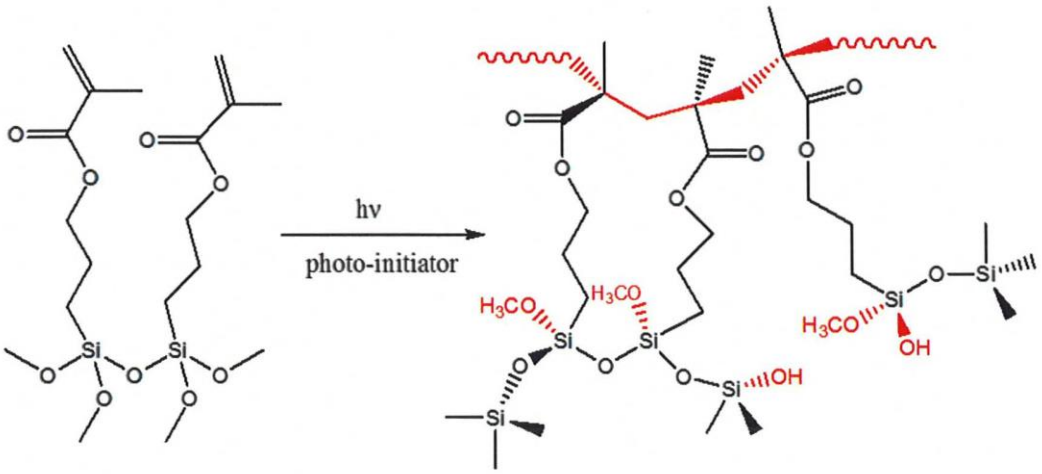

Figure 1.4 Photoinitiated free-radical polymerisation of organosiloxane with methacrylate groups. Reprinted with permission from [31].

1.1.3 Waveguide structure and the field of view (FOV)

1.1.3.1 Light propagation in a waveguide

Optical waveguide is the three-dimensional self-induced waveguide through the self-trapping of the beam, which is composed of a cylindrical core surrounding with a cladding. **Figure 1.5** is a scheme of an optical waveguide, where the refractive index of the core is n_1, while the refractive index of the cladding is n_2.

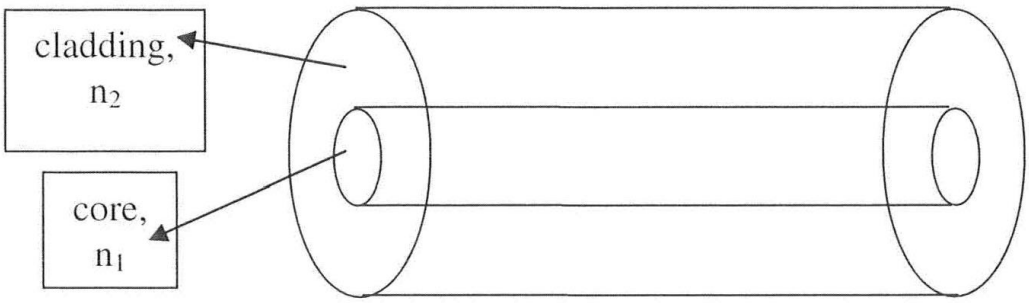

Figure 1.5 Scheme of an optical waveguide, which has a cylindrical core surrounding with a cladding. The refractive index of the core is n_1, while the refractive index of the cladding is n_2. Reprinted with permission from [31].

It's a common approach to counteract beam diffraction by using optical waveguide. For optical waveguide, the refractive index of the core is higher than the refractive index of the cladding, namely $n_1 > n_2$. However, the beam can then be confined, guided and propagated within the medium with high refractive-index due to total internal refraction. Total internal reflection is a phenomenon that the light is totally reflected when the incident angle is greater than the critical angle.[32] Based on the Snell's law, critical angle can be defined as following equation[32]:

$$\theta_{critical} = sin^{-1}(\frac{n_1}{n_2}) \qquad \textbf{1-4}$$

Therefore, total internal reflection of the light can lead it to be confined, guided and propagated within the waveguide.

1.1.3.2 The change of FOV from the waveguide structure to the waveguide-free counterparts

Basically, each waveguide has a specific angular acceptance range (i.e. FOV),

which can be illustrated as the following figure.

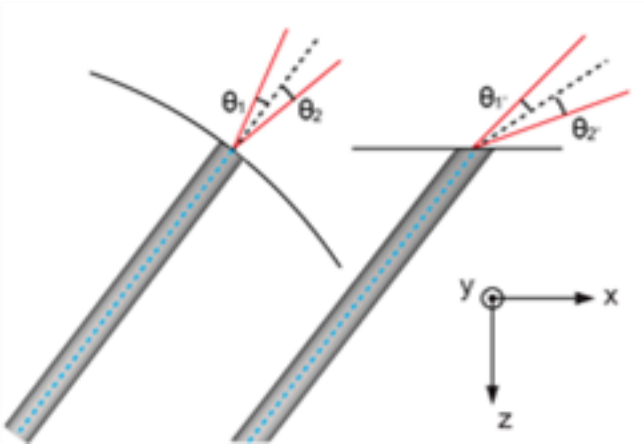

Figure 1.6 The scheme of single waveguide with specific FOV. Reprinted with permission from [33].

Comparing to the waveguide-free medium, waveguide lattices with certain arrangement could confer enhanced FOV. For the panoramic arranged waveguide lattice, the FOV of the structure is the cumulative angular ranges of each constituent waveguide[33], thus its FOV is larger than the FOV of the unstructured medium. Alternatively, the FOV of the 0-degree waveguide arrays (**Figure 1.7**) should be also broader than the waveguide-free medium. When two same beams propagate same distance, the beam intensity profile within the waveguides stays unchanged due to the self-trapping, while the beam intensity decreases due to the beam divergence in the unstructured medium.

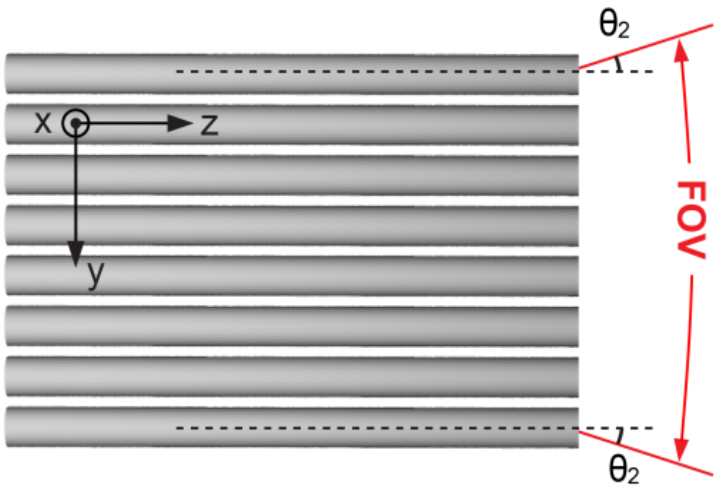

Figure 1.7 Scheme of 8 waveguides evenly spaced, which has a FOV within the y-z plane. Reprinted with permission from [33].

1.1.3.3 The continuous and discontinuous waveguide structure and their corresponding FOVs

Previous work of our group has shown that different types of compound eye-mimic structures can be created based on polymer waveguides. **Figure 1.8 (a)** is a WEL structure which has 5 lattices oriented to point different directions. Since the waveguides are arranged discontinuously, the WEL structure has a discontinuous FOV.[34] **Figure 1.8 (b)** is RDWEL structure, where the waveguides are arranged as a continuous arc, thus it has a continuous panoramic FOV.[33]

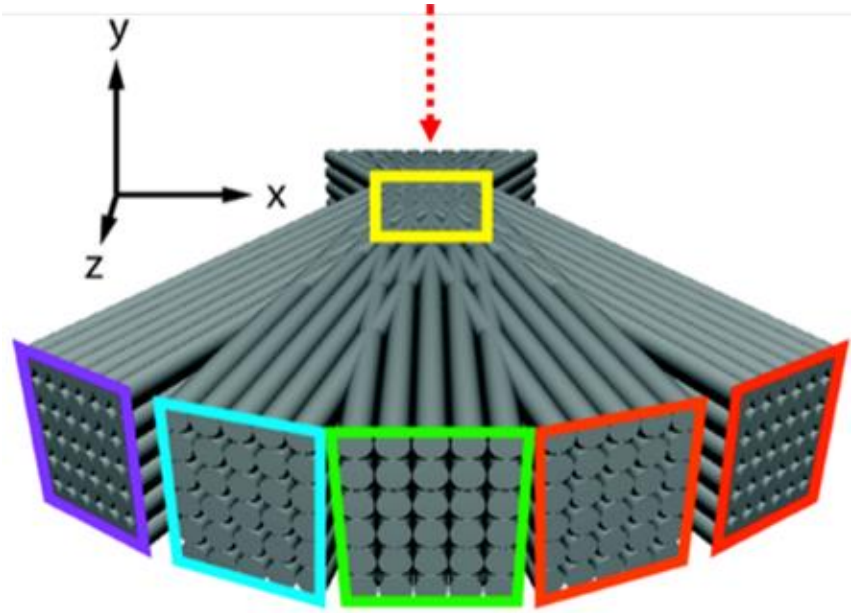

(a).

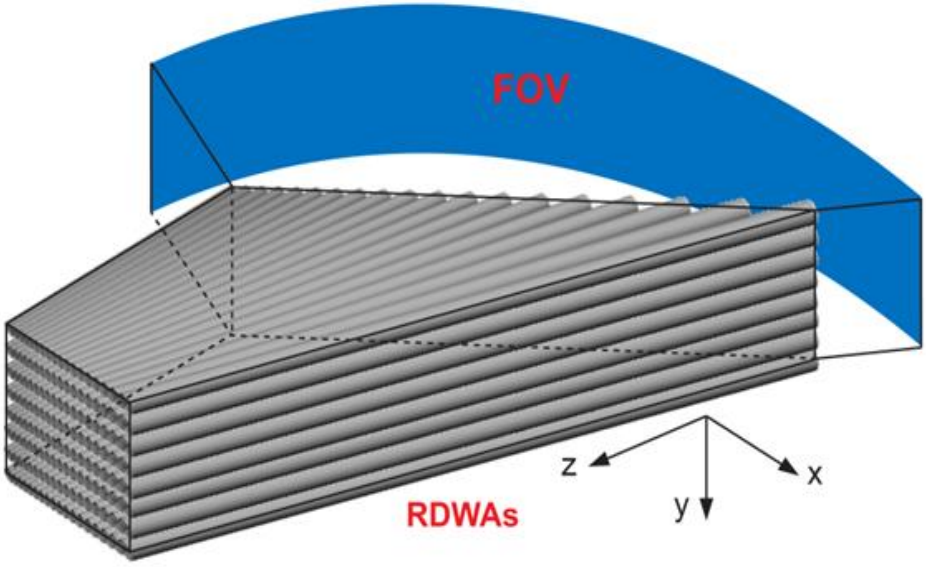

(b).

Figure 1.8 (a). scheme of the waveguide encoded lattice (WEL), which shows the extension of each waveguide array along its axis and its corresponding relative angular position. Reprinted with permission from John Wiley and Sons [34]. Copyright © 2017 Wiley-VCH Verlag GmbH & Co. KGaA, Weinheim. (b) Scheme of radially distributed waveguide encoded lattice (RDWEL) with continues panoramic FOV. Reprinted with permission from [33].

1.2 Gold nanoparticles

1.2.1 Properties of gold nanoparticles (Au NPs)

As a noble metal nanoparticle, gold nanoparticles have fabulous physical and chemical properties. Different form the bulk, the nanosized dimension of gold nanoparticles leads them to open fascinating possibilities in electronic and optical applications. Gold nanoparticles have outstanding tunability of properties, their shape, size and local environment presents can be varied under contain conditions.[35] This unusual capability provides gold nanoparticles many novel application possibilities. There are many synthesis strategies of gold nanoparticle which provides them various possibilities to incorporate into other materials. Besides, gold nanoparticles are very stable and hard to agglomerate, so they can be freely dispersed into some medium such as polymeric networks.

In particular, gold nanoparticles have strong plasmon resonance-based optical signatures, thus they have been used in various fields. Surface plasmon resonance (SPR) is one of the most outstanding physical properties of noble metal nanoparticles. The SPR can enhance the exciting electromagnetic field due to the collective oscillation of conduction band electrons on the surface of metal nanoparticles.[35] There are a wide variety of applications of SPR of gold nanoparticles[36,37], particularly in SPR sensors since they are extremely sensitive to the change in refractive index resulted from the surface plasmons.

1.2.2 Synthesis of gold nanoparticles

A variety of approaches have been developed to synthesis gold nanoparticles. One of the most general method is chemical reduction method, which consists of reduction and stabilization. Reduction agents, such as polyols, aminoboranes, are used to reduce the gold salt into element gold nanoparticles. Meanwhile, stabilization agents are used to avoid the aggregation.[38] Turkevich method[40] is one of the most classic chemical method for the synthesis of gold nanoparticles, which is based on the treatment of $HAuCl_4$ with citrate in boiling water.

Other than the common chemical synthesis, gold nanoparticles can also be synthesized through other processes, such as electrochemical method, seeding growth method, biological method etc. For this thesis work, we used the method of photoinduced *in situ* synthesis to generate the gold nanoparticles[41-43], since this method can produce the gold-polymer nanocomposite. Gold-polymer nanocomposite as metallodielectric composites combines the unique processing mechanical properties of the polymers with the outstanding physical and chemical properties of gold nanoparticles. However, it's challenging to generate a uniform distribution of gold nanoparticles within the polymeric waveguides. The synthesis mechanism is illustrated in the **Result and Discussion** section of this thesis.

1.3 Waveguide arrays doped with Au nanoparticles

1.3.1 Photoinduced *in situ* synthesis of gold-epoxide nanocomposite

As a hybrid material, noble metal nanoparticles dispersed into polymer matrix have significant potential in practical photoelectric devices due to their versatile physical and chemical properties. Particularly, epoxide-gold nanocomposite attracts more and more attentions since they have excellent chemical and thermal resistance and unique optical properties. Yagci et al. has demonstrated the *in situ* synthesis of gold-epoxy nanocomposites through photoinduced electron transfer and cationic polymerization by using visible light. [41-43]

In the work, they designed iodonium salt and $HAuCl_4$ as oxidizing agents which ensure the simultaneous generation of gold nanoparticles and cations for the cationic polymerization. The system must use two different oxidizing agents, since it requires a gold precursor and a non-nucleophilic counteranion which are impossible replaced by a single oxidizing agent. Under the illumination of visible light, the photogenerated radicals can reduce gold salt to generate gold nanoparticles. At the same time, another portion of the radicals can reduce the photoacid generator to generate the cations which can the initiate the cationic polymerization. [41]

As another research branches developed from above works, our group has modified the *in situ* synthesis method to further study modulation instability of incoherent LED beam in epoxide systems.[41] Based on the modification done by our group, this

thesis work further combined the *in situ* synthesis approach developed by Yagci et al. with a nonlinear lithographic technique to generate gold nanoparticles embedded waveguide structures for this thesis work. To be specific, we used the method of self-trapping of a broad beam of white light to fabricate large populations of epoxide waveguides containing a uniform dispersion of Au nanoparticles. The propagation of the self-trapped incoherent beams can then induce the *in situ* synthesis of gold nanoparticles and simultaneously initiate the cationic polymerization of the epoxide sols to generate the metallodielectric waveguides. The details of strategy implemented is outlined in the following as **Section 3,1**.

1.3.2 Optical properties

For the fabrication of the gold nanoparticles doped waveguides, the propagation of self-trapped white light not only induces the synthesis of gold nanoparticles, but also initiates the photopolymerization. Consequently, many gold nanoparticles are generated within the polymer waveguides. The *in situ* photogenerated gold nanoparticles can increase the localize density of the polymer waveguides, which results in the change of the refractive index.[28,44,45] Therefore, the change of refractive index is based on the loading of gold nanoparticles.

As well, since the change of refractive index is the determining factor for FOV, the increase in the change of refractive index can result in the increase of FOV. Therefore, the addition of gold nanoparticles can increase the change of refractive index and indirectly enhance the FOV. In other words, the waveguide doped with

gold nanoparticles supposes to have larger FOV comparing to the undoped waveguide.

1.4 Research objectives: Enhanced Fields of View in Waveguide Arrays doped with Au nanoparticles

Previous work[41] of our group has shown that optical polymer waveguide microstructures embedded with metal nanoparticles can be fabricated in an epoxide based photopolymerisable system by combining the *in situ* generation of metal nanoparticles with nonlinear propagation of electromagnetic field. Besides, the WEL work[34] of our group has shown that a waveguide array can collect light incident from a specific angular range. This project is based on the work mentioned above. In this work, we are working on the fabrication of an ordered array of epoxide waveguides containing a uniform dispersion of gold nanoparticles and subsequent study of their optical properties, especially the FOV. There are several specific objectives of this project as the followings.

Firstly, this project is aimed to fabricate an ordered array of 0º epoxide waveguides containing a uniform dispersion of gold nanoparticles. Since the gold-epoxide nanocomposite is going to generate as 0º waveguide arrays using incoherent white light source, it's important to select the suitable ring cells used for containing the sols, and to adjust the fabrication assembly.

After the complete of fabrication, it is valuable to study the optical properties of the gold-epoxide polymer waveguides. Since the undoped epoxide waveguide has

already shown the FOV enhancement comparing to the non-waveguide epoxide polymer, incorporating gold nanoparticle into the epoxide waveguides is going to open a fascinating possibility in the FOV. Compared to the nanoparticle-free counterparts, waveguide arrays doped with metal nanoparticles have different refractive indices, thus they possess different angular acceptance ranges (i.e. different FOV). It's valuable to compare the FOV of the epoxide waveguide doped with gold nanoparticles to the undoped waveguide, and sequentially determine the FOV enhancement.

Finally, since the optimal waveguide structures can be tuned by several fabrication conditions, we also need to examine the effects of the concentration of gold nanoparticles and the fabrication power on the FOV.

2. Experimental Section

2.1 Materials

The structures of the materials used in this study are shown in **Figure 2.1**. 3, 4-epoxycyclohexylmethyl-3', 4'-epoxycyclohexane carboxylate (ERL-4221) (**1**), poly (1, 4-butanediol (M_n 250)) (pTHF) (**2**), and camphorquinone (**3**) Epoxypropoxypropyl terminated polydimethylsiloxane (DMS) (**4**) is purchased from Gelest Inc.. Bis(4-t-butyl)iodonium hexafluroantimonate (**5**) is obtained from Hampford research Inc.. Camphorquinone is used as photosensitizer (PS) which has its peak absorption wavelength at 468 nm, and Bis(4-t-butyl)iodonium

hexafluroantimonate is used as photoinitiator (PI). (97% purity) gold (III) tetrachloride (**6**) are purchased from Sigma Aldrich (Oakville, ON). All reagents are used as received without further purification.

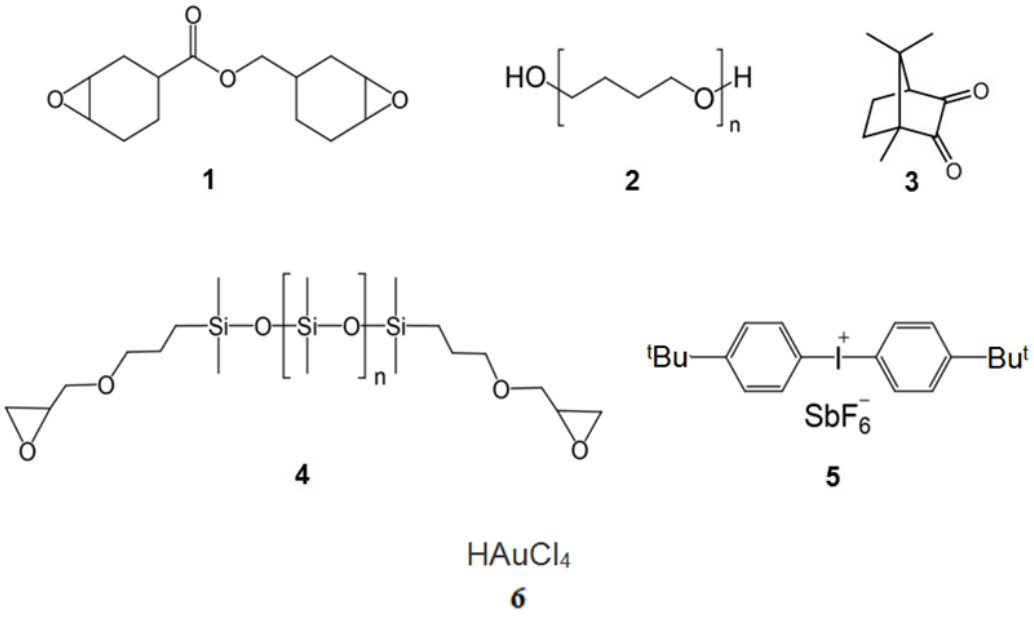

Figure 2.1 The structures of the materials used to prepare the photopolymerisable sols.

2.2 Preparation of undoped epoxide sols and the sols containing gold salts

The undoped epoxide sols were prepared by two steps. Firstly, to a reaction vial 7.6 g of ERL (76 wt%), 1.0 g of DMS (10 wt%), 0.2 g of camphorquinone (2 wt%), 0.2g of iodonium salt (2 wt%) and 1.0 g of pTHF (10 wt%) were added. The mixtures were prepared under minimal exposure to ambient light. Secondly, the entire mixtures were sealed with aluminum foil and constantly stirred for 48 hours,

followed by the filtration through a polytetrafluoroethylene filter (pore size: 0.2 μm, Pall Corporation) before use.

The epoxide sols with gold salt were prepared by the following steps. To facilitate the solubility of the gold salt in the sols, gold (III) tetrachloride was firstly mixed with pTHF. Briefly, 5 mg of gold (III) tetrachloride (0.05 wt%) was added into 0.9950 g of pTHF (9.95 wt%) and well stirred. Secondly, the gold-pTHF solution was added into a mixture containing of 7.6 g of ERL (76 wt%), 1.0 g of DMS (10 wt%), 0.2 g of camphorquinone (2 wt%) and 2g of iodonium salt (2 wt%) was prepared. All the operations were done under minimal exposure to ambient light. Finally, the resulting mixture were constantly stirred for 48 hours, followed by the filtration through a polytetrafluoroethylene filter (pore size: 0.2 μm, Pall Corporation) before use.

2.3 Preparation of experimental sols with different Au concentrations

Comparing to the undoped waveguides, the waveguides doped with different amount of gold nanoparticles may have different FOV. To study the Au-concentration dependent FOV, sols with different loading of gold salt were prepared. The weight percentages of the gold salt we selected to study were 0 wt%, 0.03 wt%, 0.04 wt% and 0.05 wt%, respectively. These sols were prepared by mixing the gold-pTHF solution with the epoxide-PS-PI mixtures as mentioned above in the general steps. Different amount of $HAuCl_4$ were dissolved in pTHF, while the total weight Au-pTHF solutions were still 1.0 g and all the weight percentage of other chemical

components were kept constant. Same as the general preparation steps, these sols were prevented from exposure to ambient light, constantly stirred for 48 hours and filtered before being used.

2.4 Optical assembly for structure fabrication

Figure 2.2 shows the optical assembly used to fabricate the 0° epoxide-based metallodielectric and dielectric waveguide arrays. A broad beam of white incandescent light (320-800 nm) was generated from a quartz tungsten halogen lamp (QTH) (Cole-Parmer). The beam was collimated by a planoconvex lens L_1 (F. L. = 250 mm) then passed through an optical photo-mask (PhotomaskPORTAL, square grid pattern, periodicity = 40 μm) before launched onto the entrance face of the sample cell (Diameter = 16 mm, path length = 2 mm) containing the photopolymerisable sol. The beam intensity profiles at the exit face of the sample ring cell were captured using a pair of planoconvex lenses L_2 and L_3 (F. L. = 250 mm) and focused onto a high-resolution, progressive scan, charged-coupled device (CCD) (1360 (H) x 1024 (V) 3.2 μm square pixels, sensitivity range = 350 nm to 1150 nm; WinCamDTM digital camera, Data Ray Inc., USA). Both the photomask and the sample cell were assembled on a rotation stage, and all the optical components and the rotation were mounted on a linear optical rail (resolution = 1mm) with rail carriers,

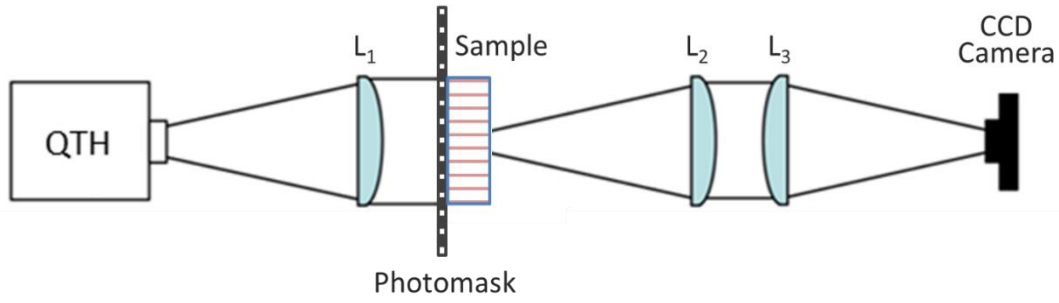

Figure 2.2 Schematic diagram of optical setup used to fabricate the 0˚ array of epoxide-based metallodielectric and dielectric waveguides.

2.5 Fabrication conditions of the structures

Since the fabrication exposure power may affect the resulting structure, both 7.0 mW and 8.0 mW were used for the fabrication. Power was measured at the entrance face of the photomask using a power meter, and the power meter was set to 468 nm since the absorption peak of camphorquinone is at 468 nm. The evolution of reaction was monitored with the CCD camera, and the beam intensity profiles at the exit face of the samples were recorded every 60s. Since the sols loaded with different amount of the gold salt have different transparency, the illumination time needed to fabricate these structures may vary. Multiple experiments were done to optimize the fabrication time of the structures with different amount of gold salt. To be specific, when illuminated under a 7.0 mW white incandescent lamp, the epoxide sols containing 0 wt% (the undoped sols), 0.03 wt%, 0.04 wt% and 0.05 wt% gold salt were irradiated for 48, 50, 52, 58 minutes respectively. However, when illuminated under an 8.0 mW white incandescent lamp, the epoxide sols containing 0 wt% (the undoped sols), 0.03 wt%, and 0.05 wt% gold salt were

irradiated for 30, 33, 35 minutes respectively.

2.6 Structural Characterization

Laser transmission images of the waveguides doped with gold nanoparticles and the undoped waveguides obtained with a He-Ne laser (632.8 nm, Spectra-Physics, USA). The micrographs of the structures were captured using an Olympus BX51 optical microscope (×5 magnification), fitted with a Q-Imaging Retiga EXi digital camera and Image proTM software. From previous work done by Dr. D. K. Basker, the JEOL 2010F field emission transmission electron microscopy (TEM) equipped with energy dispersive X-ray spectroscopy (EDS) spectrometer was used to characterize the metal nanoparticles. Samples for the TEM was prepared using ultramicrotome and sliced to about 70 nm.

2.7 FOVs measurements

Figure 2.3a shows the schematic diagram of the optical assembly used for measuring the FOV of the waveguide arrays. The photograph of the actual setup is shown in **Figure 2.3b** (All optical components are labeled corresponding to that in **Figure 2.3**). A broad collimated beam of white light generated from a QTH lamp (Ocean Optic Inc.) and passing through a donut shaped mask (~3 mm) was used as the probe beam. The fabricated waveguide samples (S) were mounted on a rotation strage (R), which was rotatable around the vertical y-axis with a resolution of 1°. An aperture (A) was placed in front of a pair of planoconvex lenses L_2 and L_3 (F.

L. = 250 mm, diameter D= 25.4 mm) to block the stray light. All imaging components were mounted on an optical linear rail (resolution = 1mm) and to vary the incident angle of the probe beam, the optical rail was rotated ± 8° about the optical axis of the beam with an interval of 0.5°. The intensity profile at the exit face of the testing samples under each incident angle were captured by a CCD camera (1360 (H) x 1024 (V) of 3.2 µm square pixels, sensitivity range = 350 nm to 1150 nm; WinCamDTM digital camera, Data Ray Inc., USA). Three or more parallel experiments were done for each waveguide array with different concentration of gold nanoparticles to ensure accuracy.

a

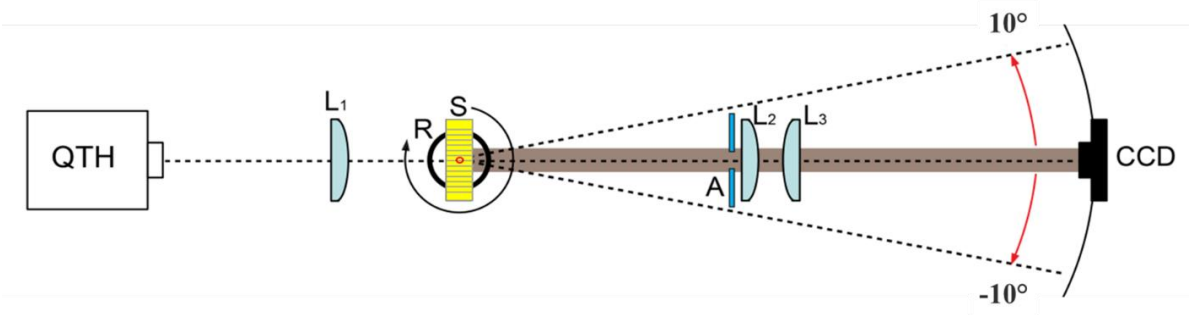

b

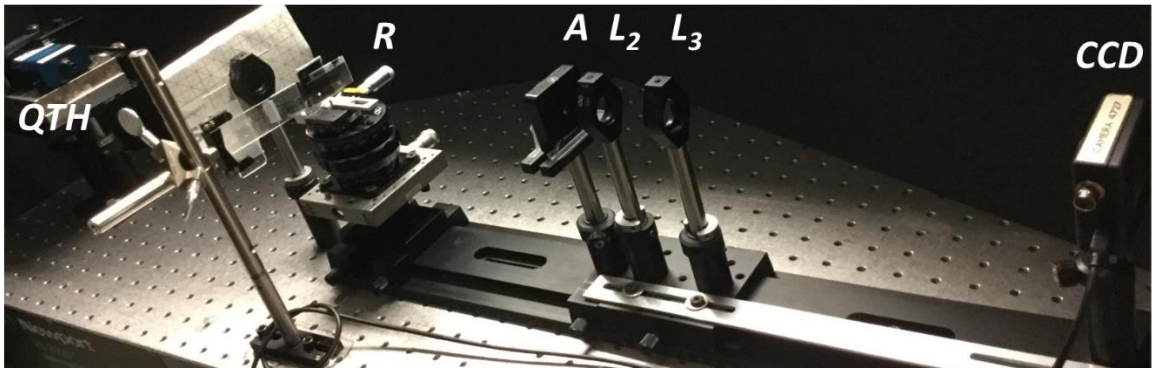

Figure 2.3 a) Scheme of optical assembly for measuring the FOV of the waveguides.

b) Photograph of the actual setup used for measuring the FOV.

3. Results and discussion

3.1 Photoinduced *in situ* synthesis of epoxide-metal nanocomposite

The epoxide photopolymerization system with the *in situ* gold nanoparticle synthesis was developed by Yagci et al.[41-43] We combined the *in situ* synthesis approach developed by Yagci et al. with the self-trapping[1] of a broad beam of white light for fabricating gold nanoparticles embedded waveguide structures. In other words, we developed a nonlinear lithographic technique to generate large populations of epoxide waveguides containing a uniform dispersion of Au nanoparticles. The method is based on the self-trapping[46] of a broad beam of white light propagating through a cationic polymerizable matrix doped with the $HAuCl_4$, which initiates the polymerization of epoxide moieties to form waveguides while simultaneously *in situ* synthesizes of elemental Au nanoparticles.[47]

To generate gold nanoparticles embedded epoxide waveguide structures, $HAuCl_4$, camphorquinone (visible light sensitizer) and bis(4-t-butyl)iodonium hexafluroantimonate (photoacid generator) are used to enable the cationic chain propagation of metallodielectric epoxide polymer. **Figure 2.4** shows the mechanism of visible light induced *in situ* synthesis of the element gold nanoparticles and the simultaneously cationic polymerization of epoxide moieties. Upon exposure to visible light, camphorequinone absorbs the photon energy to form camphorquinone radicals (i.e. step 1 in Figure 5). A portion of photogenerated camphorquinone radicals then react with $HAuCl_4$ and reduce it to zero-valent nano

scale gold and achieve the *in situ* synthesis of gold nanoparticles (i.e. step 2 in **Figure 2.4**). The formation of epoxide waveguides occurs simultaneously as the formation of the gold nanoparticles. The chain propagation is induced by cationic polymerization. However, the cationic polymerization of epoxide moieties cannot be enabled by $HAuCl_4$ which does not carry non-nucleophilic counteranion. In other words, the oxidant used to generate the initiating cations of the polymerization is different from the one for the *in situ* synthesis of Au nanoparticles. The mechanism of the cationic polymerization can be illustrated as the following. The other portion of photogenerated camphorquinone radicals (in setp 1) are oxidized by bis(4-t-butyl)iodonium hexafluroantimonate to form H^+X^- (Step 3), which reacts with epoxide monomers to generate an initiative epoxide cation (step 4), then starts the polymer chain propagation (Step 5).

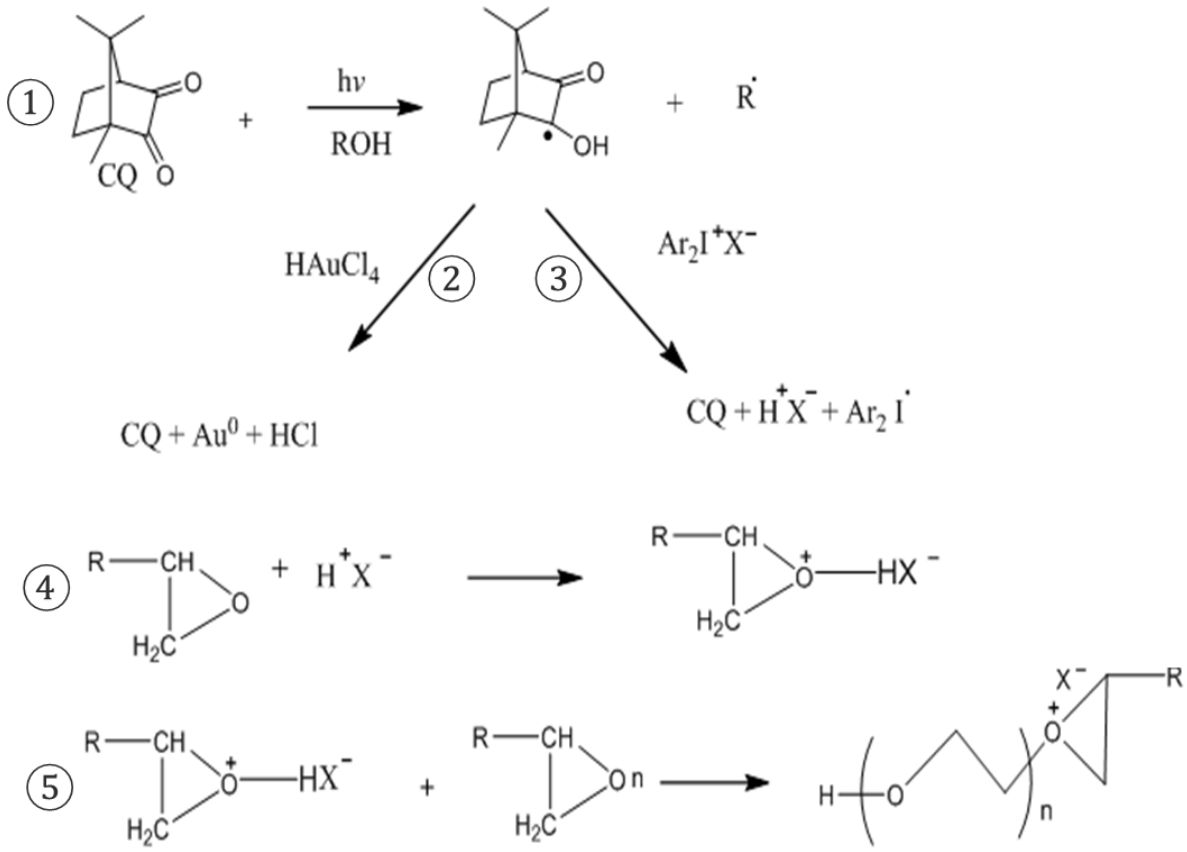

Figure 2.4 Mechanism for visible light induced *in situ* synthesis of gold-epoxide and the simultaneously cationic polymerization of epoxide moieties. Reprinted with permission from [44].

3.2 Sample appearance

Figure 3.1 shows the appearance of the experimentally fabricated undoped waveguide samples and the corresponding samples doped with gold nanoparticles. As we can see, the sample with its waveguide doped with gold nanoparticles has dark brown color while the undoped waveguide sample is yellow (due to un-reacted camphorquinone), which can preliminary indicate that gold nanoparticles were generated during illumination.

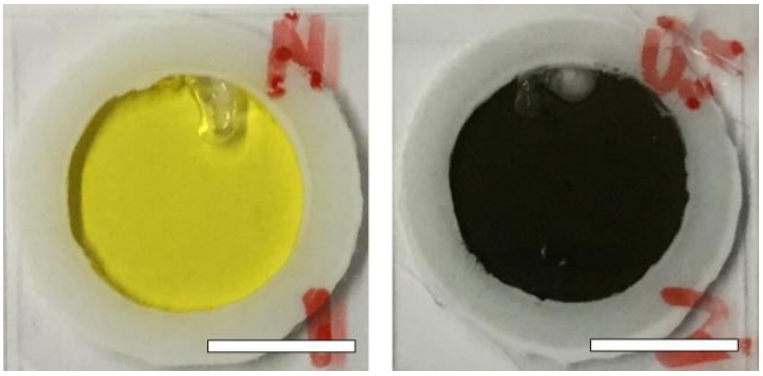

Figure 3.1. Comparison of the appearance of the actual samples experimentally fabricated. The structure of undoped waveguide is shown on the left and waveguide-encoded sample doped with Au NPs is shown on the right. (Scale bar = 1mm).

3.3 Optical characterization of the waveguide matrix structure

During the illumination, the photoinitiated ring opening cationic polymerization took place, which resulted in the increase of the localize density and the corresponding change in the refractive index. [28,44,45] The photomask could lead the uniform broad beam to split into individual narrow self-trapped filaments. The self-trapped beams then inscribed permanent cylindrical structures along their path during the irreversible polymerization, which led to the formation of the waveguides. For this project, since we didn't put any condenser lens in front of the samples, the generated waveguides are 0° and periodically spaced, a scheme of the matrix structure is shown in **Figure 3.2.**

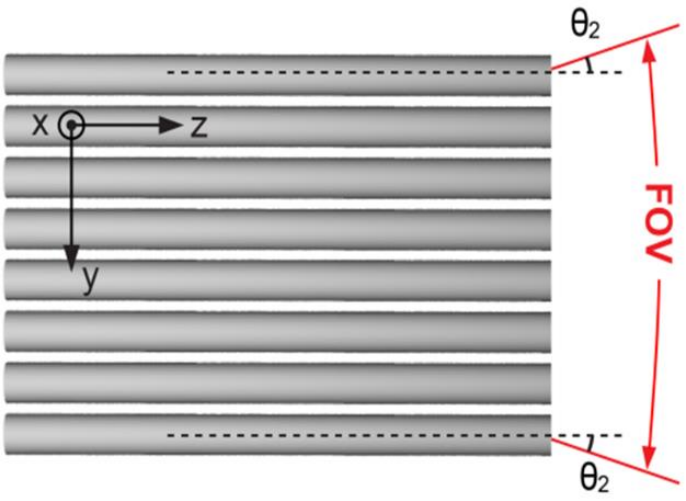

Figure 3.2 Scheme of 8 waveguides evenly spaced, which has a FOV within the y-z plane.

The laser transmission profiles and the optical micrographs of the transverse cross-sections of the waveguide sample are shown as **Figure 3.3**. It's clear that all images exhibit periodically spaced high intensity spots, which refer to waveguides. Those are the evidence of the formation of the 0° waveguide arrays.

a.

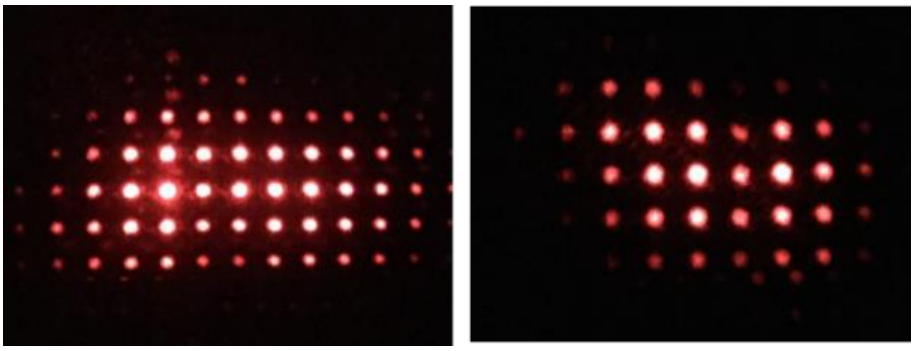

b.

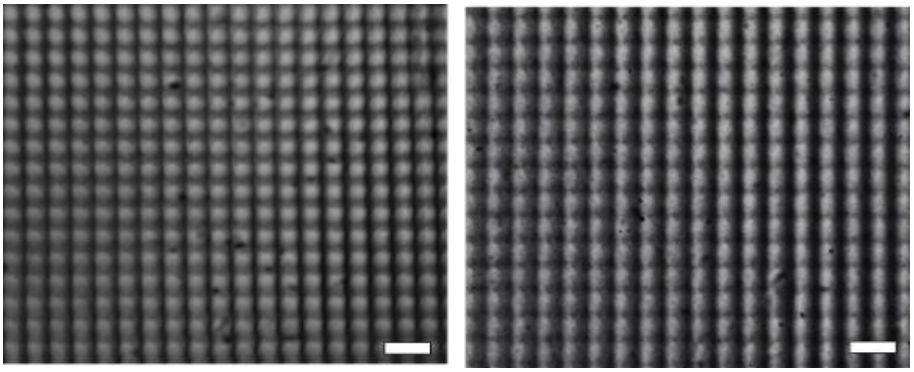

Figure 3.3 The optical characterizations for the 0° waveguide arrays. a) Laser transmission profiles of the transverse cross-sections of the undoped waveguide array (left) and the waveguide array doped with Au nanopaticles (right). (Scale bar = 160 μm). b) Optical transmission micrographs of the transverse cross-sections of the undoped waveguide array (left) and the waveguide lattice doped with Au nanoparticles (right). (Scale bar = 160 μm).

From all the transverse cross-section images above of the undoped waveguide and the waveguide doped with Au nanoparticles, the presence of the spots indicates that the waveguides were imaged straight on. Therefore, the 0° metallodielectric and dielectric waveguides were formed.

3.4 Characterization of the gold nanoparticles

For the sol with gold salt, as the white light self-trapped to induce the inscription of the waveguides, the *in situ* generation of metal nanoparticles is also taking place. As mentioned in **Section 3.1**, the *in situ* synthesis of gold nanoparticles is photoinduced, so most of the generated gold nanoparticles should distribute in the core of the cylindrical waveguides, as shown in the scheme in **Figure 3.4**.

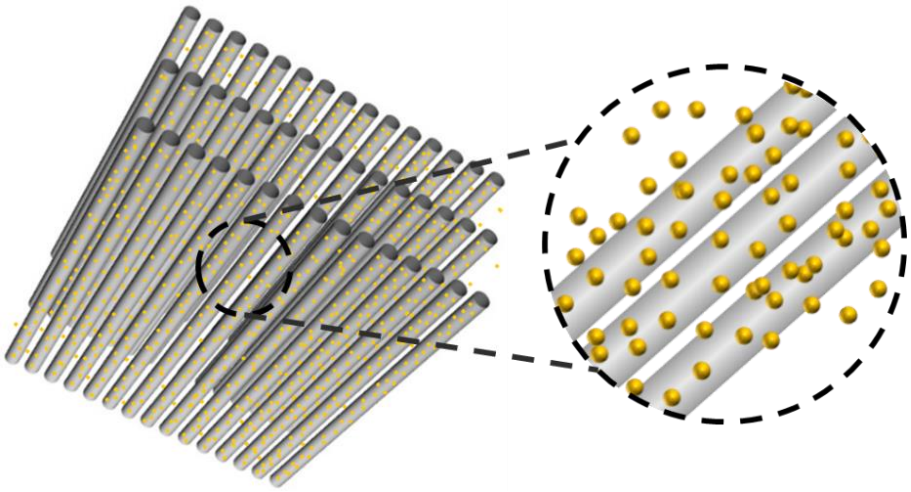

Figure 3.4 Scheme of the 0º epoxide waveguide arrays doped with gold nanoparticles

Previous work of our group has characterized the generation of gold nanoparticles, that we conducted TEM microscopy and EDX spectroscopy to ultrathin waveguide samples doped with gold salt. The EDX spectrum in **Figure 3.5c** shows strong peak of Au, indicating the existence of elemental gold in the structure. The TEM micrographs in Figure 11a-b shows the morphology of the gold, which indicate that the elemental gold is in the form of spherical gold nanoparticles, with average diameter of 10 ± 3 nm. **Figure 3.5d** shows the Ultraviolet–visible **(**UV-vis) spectrum of the waveguide structure embedded with gold nanoparticles. It exhibits a peak absorption wavelength at 560 nm, which corresponds to the dipolar plasmon resonance of gold nanoparticles embedded in polymers.

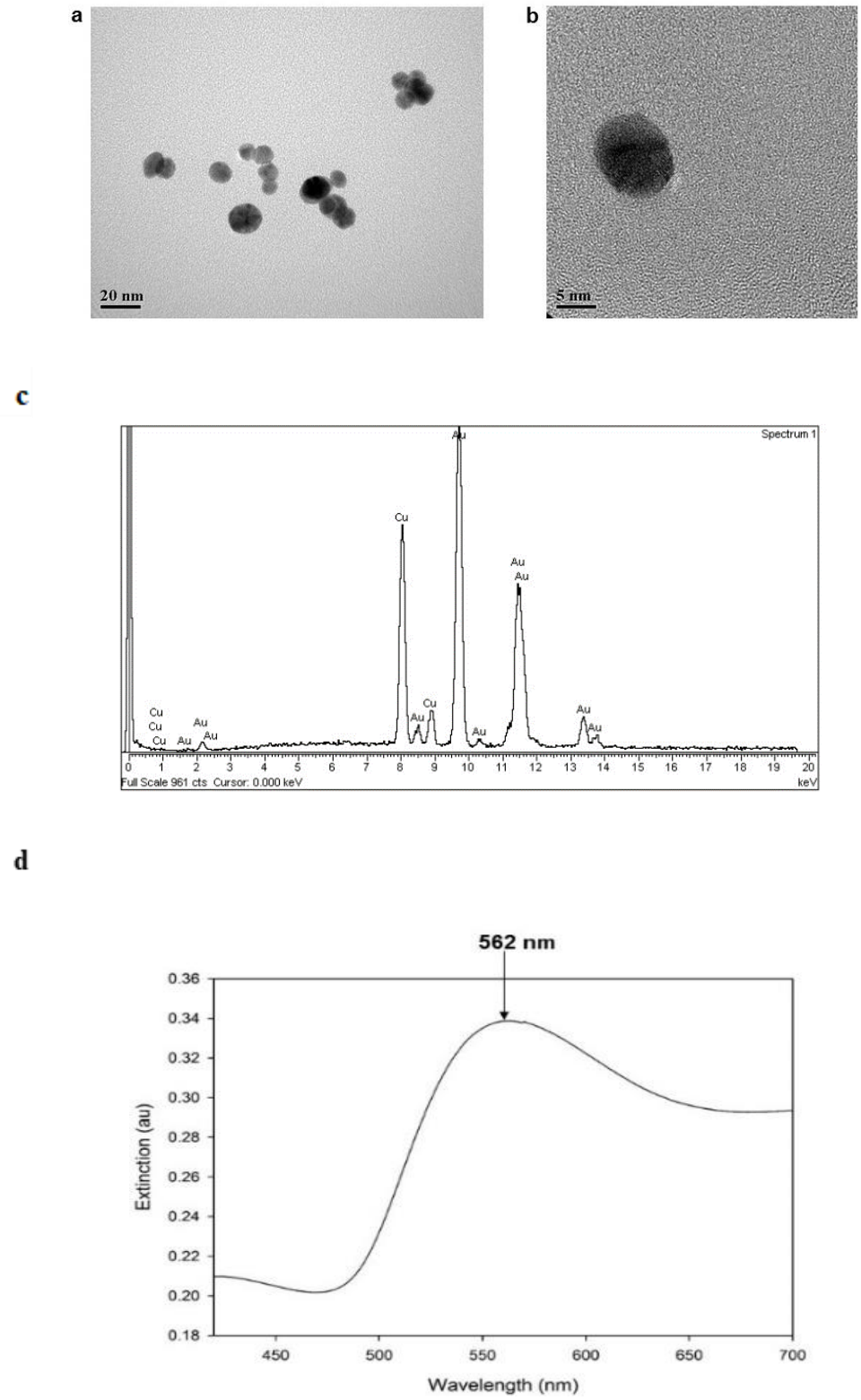

Figure 3.5 The optical characterizations for gold nanoparticles. a) The TEM

micrographs which shows the distribution of Au nanoparticles in epoxide waveguide arrays. b) high resolution TEM image showing the presence of single gold nanoparticle. c) EDX spectrum confirming the presence of elemental gold. d) UV-Vis absorption spectrum of a waveguide structure embedded with gold nanoparticles. Reprinted with permission from [44].

3.5 The enhanced FOV

Previous work of my group shows that the 0° waveguides set of the RDWEL structures had larger angular acceptance range than the 0° control sample (i.e. waveguide-free medium). In this project, the FOV measurements were done for the 0° epoxide waveguide array doped with gold nanoparticles, 0° undoped epoxide waveguide array, and the control sample (i.e., the waveguide-free epoxide sol). **Figure 3.6** compares the acceptance patterns of the 0° waveguide array doped with gold nanoparticles, 0° undoped waveguide array and control sample (waveguide-free sample). For each acceptance pattern, each donut image represents the intensity profile at the exit face of the testing sample under each incident angle, where the incidence angle was varied from −6° to 6°. All these tree patterns show that the intensity of the donut image drops as the incident angle of the probe beam increases. By comparing all the acceptance patterns, it is obvious that the 0° waveguide array doped with gold nanoparticles has the largest acceptance range while the control sample has the least acceptance range. To clarify, the patterns of the waveguides doped with Au nanoparticles in **Figure 3.6** should have lowest intensities comparing to other two patterns, due to the absorption and scattering of the generated Au nanoparticles. However, higher exposure time was used for the

measurements for the Au nanoparticles doped structures, which lets the pattern shows higher intensity.

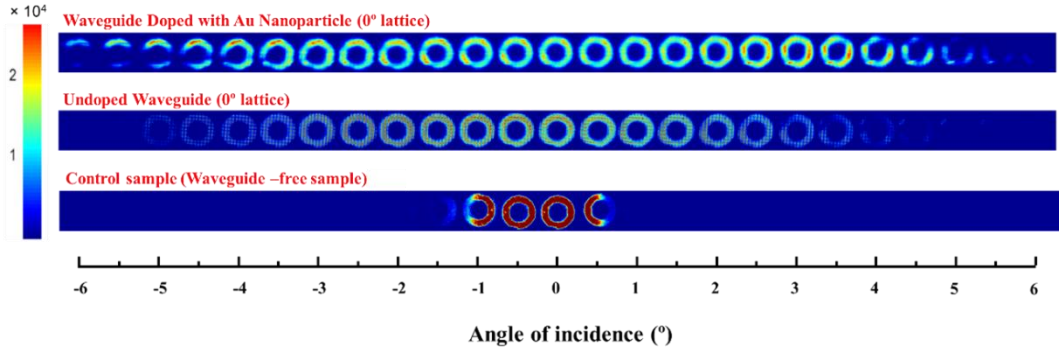

Figure 3.6. Comparison of the acceptance patterns among the 0° waveguide array doped with gold nanoparticles (top), the 0° undoped waveguide array (medium) and the control sample (bottom). For each acceptance pattern, each donut image represents the intensity profile at the exit face of the testing sample under each incident angle, where the incidence angle was varied from −6° to 6°.

The intensity profile was in donut shape since it is easier for the following integration for FOV quatification. To quantify the enhancement in the FOV for the 0° waveguide array doped with gold nanoparticles, the total intensities of the images in all acceptance patterns of **Figure 3.6** were integrated, normalized to the highest values and plotted against the incident angles. **Figure 3.7** shows the plots obtained from the 0° waveguides array (red), the 0° waveguides array doped with gold nanoparticles (black) and the waveguide-free control samples (blue).

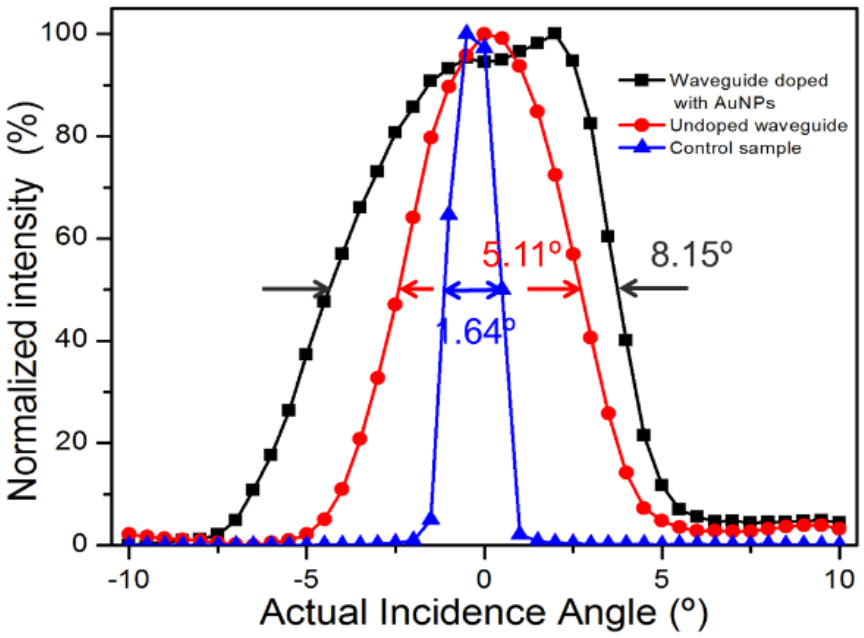

Figure 3.7 Comparison of the FOV among the 0° waveguide array doped with gold nanoparticles (black), the 0° undoped waveguide array (red) and the control sample without waveguide (blue).

It is obvious that both structures with waveguide arrays have much larger acceptance range than the waveguide-free medium (i.e. the epoxide sol). The FOV of a structure is determined by the full width at half maximum (FWHM) of the corresponding plot. Therefore, it was found that 0° undoped epoxide waveguide array, the 0° epoxide waveguide array doped with gold nanoparticles and the 0° waveguide-free medium have FOV of 5.11°, 8.15° and 1.64° respectively. Compared to the 0° waveguide-free medium, the 0° undoped epoxide waveguide exhibits an enhancement of ~212% in FOV (as **Figure 3.8a**), while the 0° waveguide doped with gold nanoparticles exhibits an enhancement of ~397% (as **Figure 3.8b**). Comparing the FOV of the two waveguide structures, we can see that

after introduced with Au nanoparticles, the FOV was increased by ~59% (as **Figure 3.8c**).

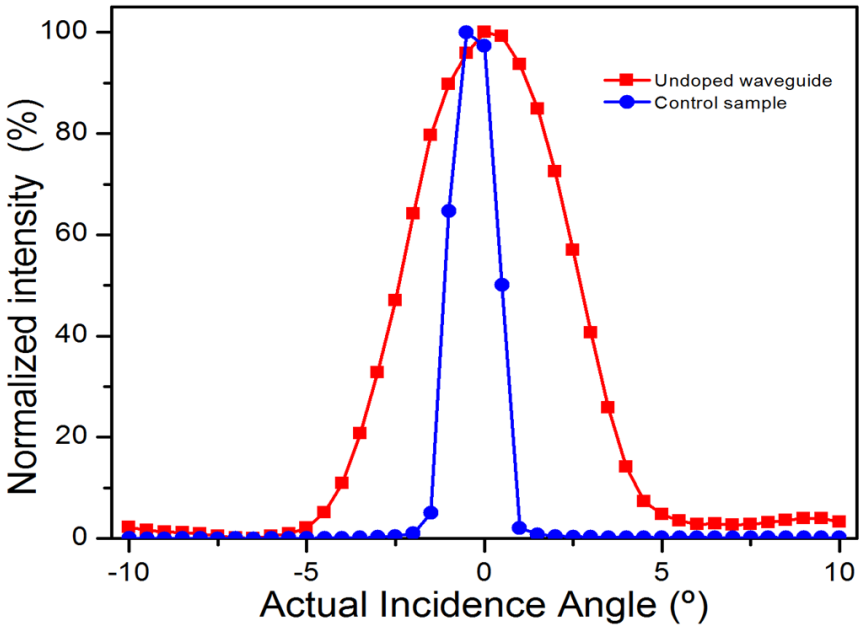

a.

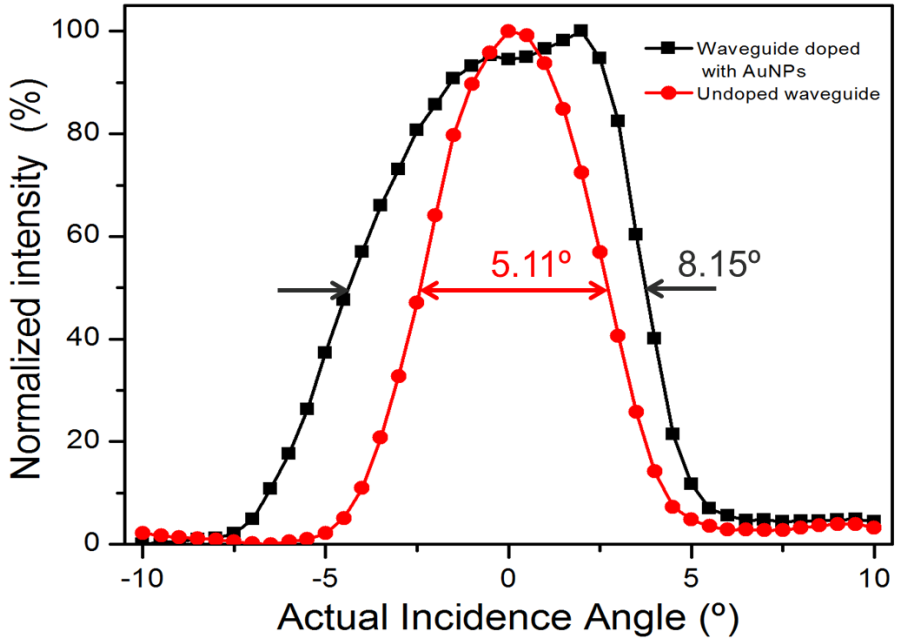

b.

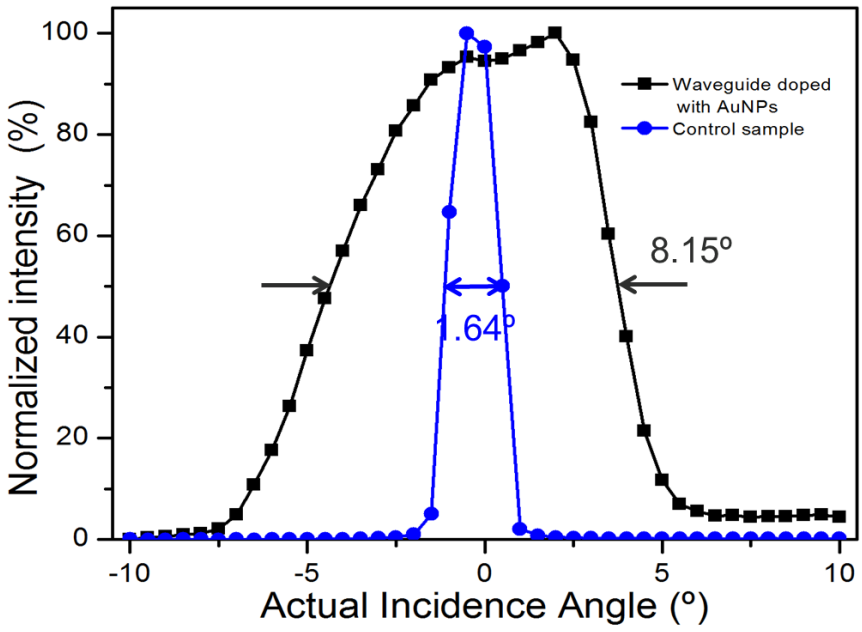

c. **d.**

Figure 3.8 (a) Comparison of the FOV between the undoped waveguide array (red) and the control sample (i.e. waveguide-free medium) (blue). (b) Comparison of the FOV between the waveguide array doped with Au NPs (black) and the undoped waveguide array (red). (c) Comparison of the FOV between the waveguide array doped with Au NPs (black) and the control sample (i.e. waveguide-free medium) (blue).

Both **Figure 3.6** and **Figure 3.8c** indicate that the 0° waveguide doped with gold nanoparticles is more efficient than the 0° undoped waveguide on collecting and guiding light with larger incident angles. The waveguide doped with gold nanoparticles has broader FOV.

3.6 Au concentration dependent FOV

The FOV plots of the waveguide arrays doped with different amount of gold salt are shown in **Figure 3.9a, c**. The resulting FOV values are plotted versus gold

concentration, as shown in **Figure 3.9b, d** respectively. It is very clear that the FOV values of the 0° waveguide array enlarges as the increasing load of gold salt, that following an exponential trend. We can then deduce that, with even heavier loading of gold salt, even larger FOV will be achieved. However, the conclusion only applies on the waveguide arrays doped with 0 to 0.05 wt% gold nanoparticles, since the 0.05 wt% nanoparticles is the upper limit for the gold concentration. Furthermore, for the waveguides doped more than 0.05 wt% nanoparticles, it is impossible to measure the FOV, since the light intensity is too low to be captured due to the light absorption of gold nanoparticle.

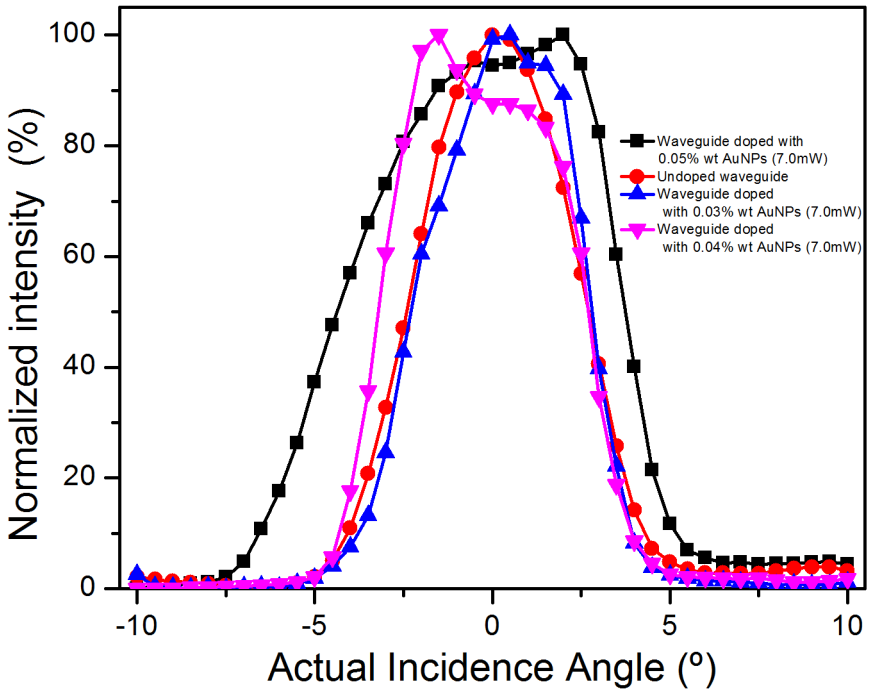

a.

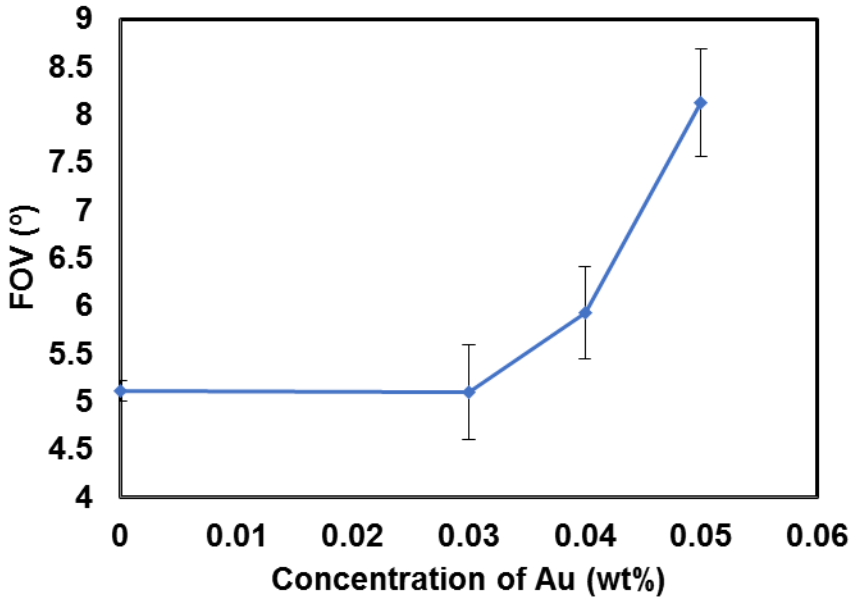
FOV (°)
9
8.5
8
7.5
7
6.5
6
5.5
5
4.5
4
0
0.01
0.02
0.03
0.04
0.05
0.06
Concentration of Au (wt%)

b.

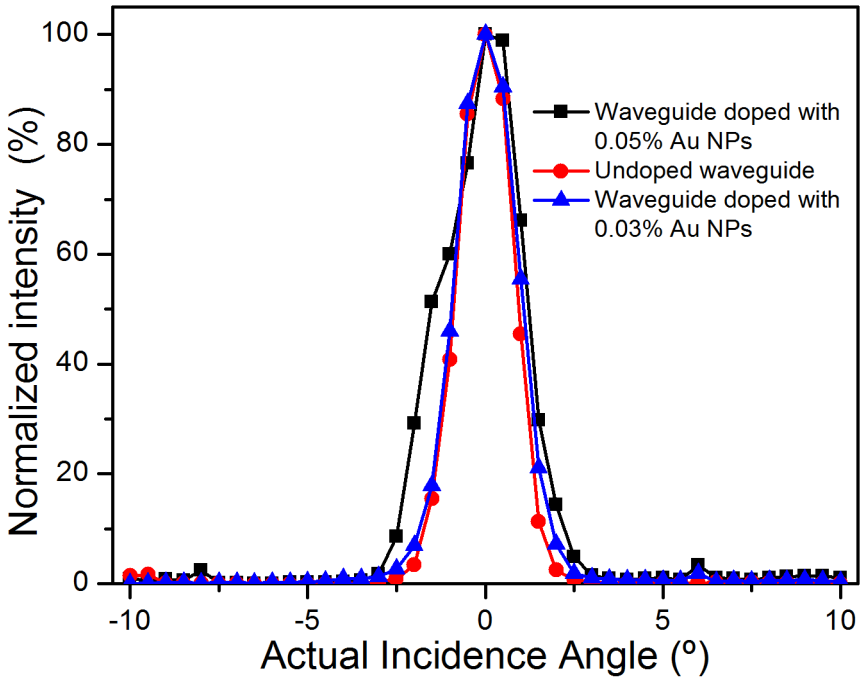
Normalized intensity (%)
100
80
60
40
20
0
-10
-5
0
5
10
Actual Incidence Angle (°)
Waveguide doped with 0.05% Au NPs
Undoped waveguide
Waveguide doped with 0.03% Au NPs

c.

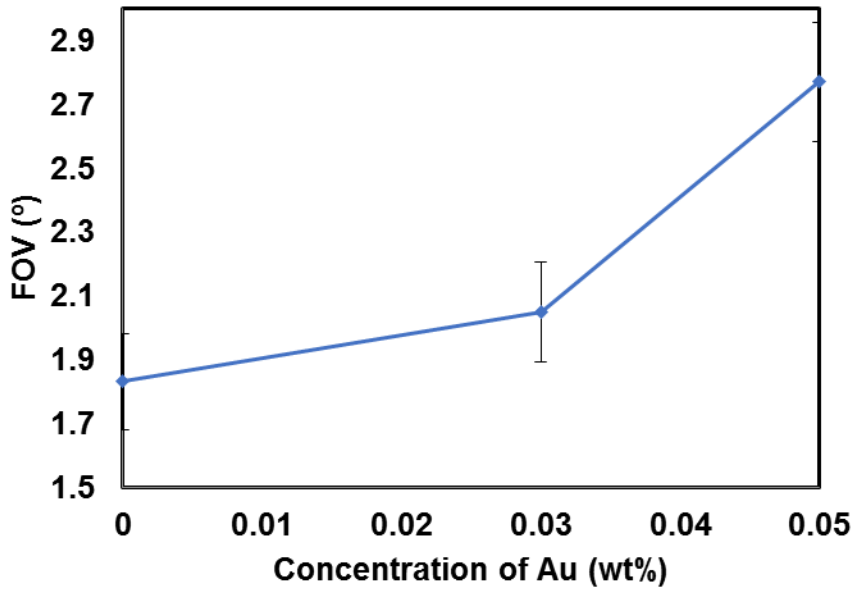

d.

Figure 3.9 a) Comparison of the FOV plots of waveguide arrays doped with different amount of gold salt. (For the waveguides fabricated under 7.0 mW illumination). b) The plot of gold concentration dependent FOV (For the waveguides fabricated under 7.0 mW illumination). c) Comparison of the FOV plots of waveguide arrays doped with different amount of gold salt (For the waveguides fabricated under 8.0 mW illumination). d) The plot of gold concentration dependent FOV. (For the waveguides fabricated under 8.0 mW illumination)

3.7 Au concentration dependent Δn

The addition of the gold nanoparticles leads to the change of refractive index. Since the change of refractive index is the determining factor for FOV, it's valuable to study the relationship between Δn and the gold concentration. The FOV is positive related with Δn of a material. To study the relationship between the Δn and the concentration of gold nanoparticle, the resulting FOV values are plotted versus the Δn which is shown a **Figure 3.10**, where the FOV is determined at the full width at

$1/e^2$ of the corresponding plot. Based on **Figure 3.10**, Δn under different Au concentration can be determined and shown as graph b. Then the plot of Δn versus concentration is deducted as shown in **Figure 3.11**.

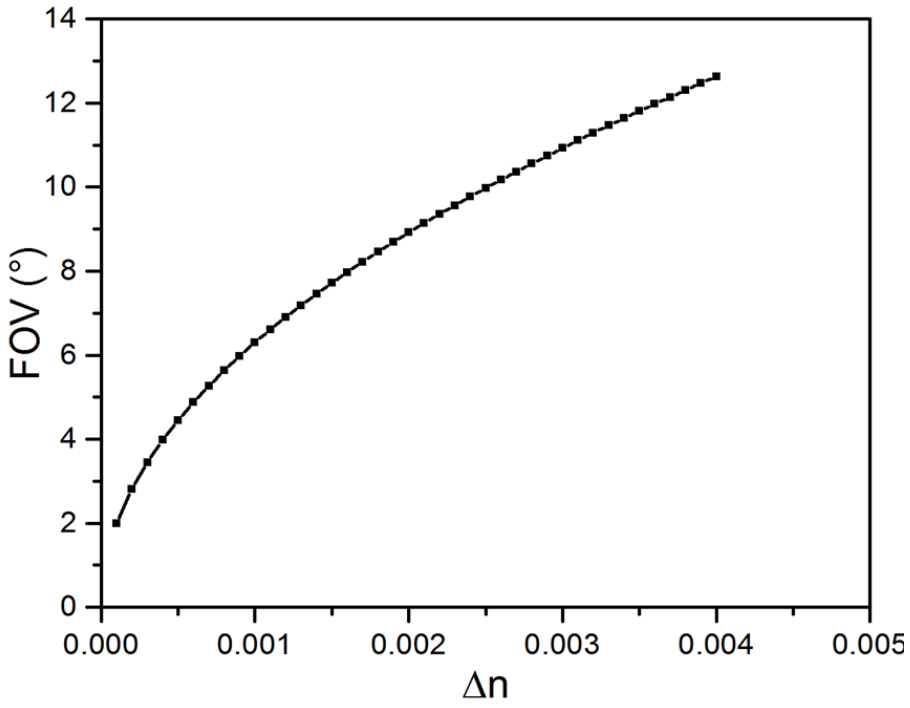

Figure 3.10 The relationship between the FOV and the change of refractive index

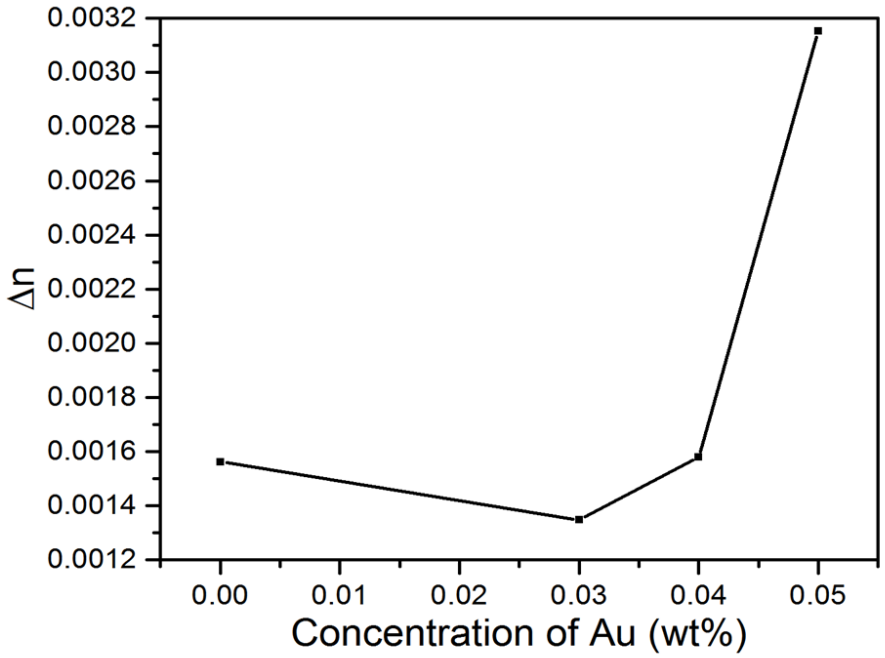

Figure 3.11 The plot of gold concentration dependent Δn (The structures are all fabricated under 7.0 mW illumination).

3.8 The effect of fabrication power on FOV

The structures fabricated at 7.0 mW exhibit much larger FOV (**Figure3.11 b,d**), therefore the FOVs of the gold-epoxide waveguide arrays are assumed to be dependent on the fabrication power. According to the assumption, a study of fabrication power dependent FOV was carried out. Please notice that both the lamp as light source and the sensor of power meter were changed to new ones for the study of the effect of fabrication power on FOV, so the intensity reading for this section are not exactly agree with previous results. However, all the experiments were done after the calibration of the equipment, thus the tendencies concluded from the concentration dependent FOV study are still correct. **Figure 3.11a-c** shows

the relationship between the FOV and the fabrication intensity, and the amount of gold nanoparticles doped keeps consistent for each plot. The results clearly show that the optimum fabrication power is at 10mW.

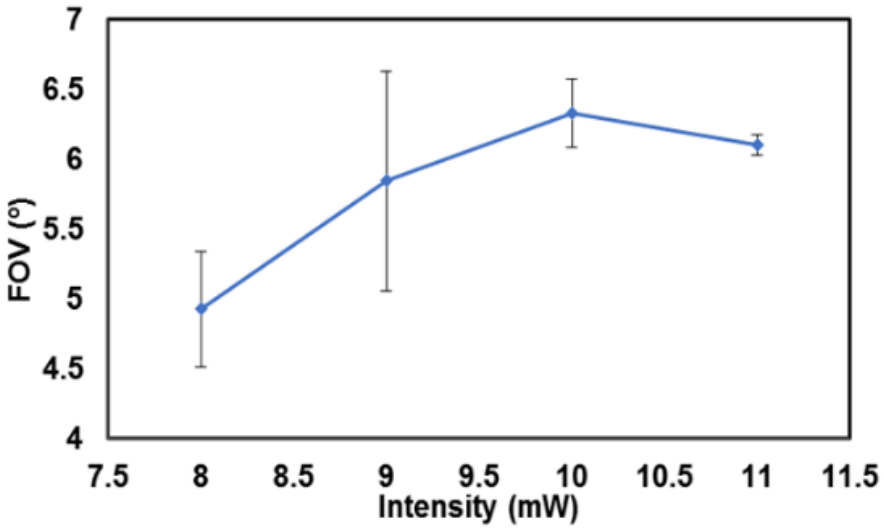

a.

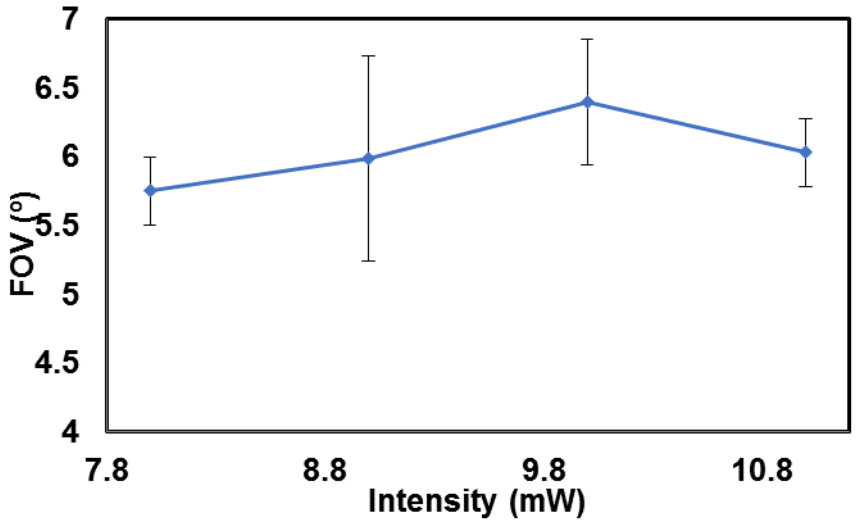

b.

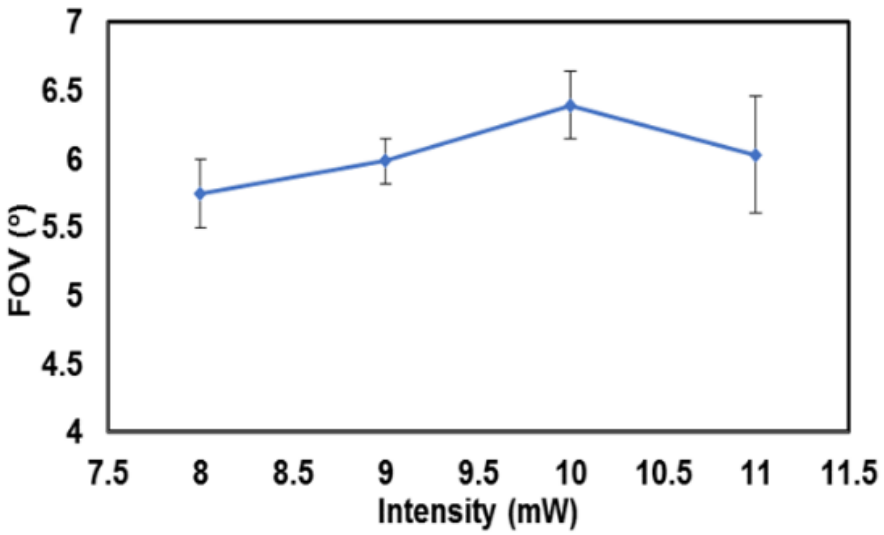

c.

Figure 3.12 The plots of fabrication power dependent FOV a) The plot of the waveguides doped with 0.03 wt% Au nanoparticles. b) The plot of the waveguides doped with 0.04 wt% Au nanoparticles. c) The plot of the waveguides doped with 0.05 wt% Au nanoparticles.

4. Conclusions

In summary, an array of polymer waveguides doped with a dispersion of Au nanoparticles is fabricated by propagating a broad beam of white incandescent light into an epoxide-based photo-polymerizable medium doped with gold salt ($HAuCl_4$). The broad beam of white light launched into this hybrid medium spontaneously break into microscopic filaments, which not only initiate the cationic polymerization of epoxide monomers to form waveguides but also simultaneously induce the electron transfer for the *in situ* reduction synthesis of Au nanoparticles. Therefore, most of Au nanoparticles distribute in the cores of the metalldielectric waveguide array, which provide the polymer matrices with strong plasmon resonance-based optical signatures. The FOV measurements indicate that the metallodielectric waveguide array fabricated has a significantly nearly 59% increase in the FOV relative to their all-dielectric counterparts. In addition, the FOV of metallodielectric waveguide array can be tuned through the concentration of Au nanoparticles and the optical intensities employed to generate waveguides. The study of gold concentration depended FOV indicates that the corresponding FOV is enlarged as the concentration of gold nanoparticles increases. As well, the study of fabrication power depended FOV indicates that the optimum fabrication intensity is 10mW.

5. Possible Future Works

According to this thesis work, we propose the future works in several directions.

For the waveguides doped less than 0.05 wt% gold nanoparticles, the heavier loading of gold nanoparticle in the metallodielectric waveguides can results in larger refractive index and corresponding larger FOV, so the large FOV is ensured by stable and uniform dispersion of metal nanoparticles within the metallodielectric waveguides. Currently, we can *in situ* synthesis the gold-epoxide waveguides, however the gold nanoparticles are randomly distributing in the waveguides. Therefore, the further study can modify the fabrication method to precisely control the microstructure of the metallodielectric waveguide arrays. It's important to make sure that the gold nanoparticles are stable and dispersing uniform within the waveguides. In addition, it's important to make sure that the gold nanoparticles are mainly fixing inside the waveguides, which means that the population of gold nanoparticles generated within the waveguides arrays is much larger than the surrounding's.

It's also necessary to measure TEM micrographs of the metallodielectric waveguides to optical characterize the size and the distribution of the gold nanoparticles. Previous work of our group has measured the TEM micrographs of the epoxide doped with gold nanoparticles[41] which shown that the existence of Au nanoparticles within the waveguides. However, comparing to the previous work, this thesis work uses different compositions of gold-epoxide system as well as

different fabrication methods including different light source, different fabrication power and different fabrication setup, so the microstructures of the resulting metallodielectric waveguides are different too. Thus, it's also necessary to measure TEM micrographs for the metallodielectric waveguides of this thesis work to determine the size and characterize the distribution of the gold nanoparticles within the waveguides. Especially, for the future work mentioned in the previous paragraph, TEM micrograph can be a powerful evidence of the uniform dispersion of metal nanoparticles within the waveguides.

Since this thesis work only considered the 0° waveguides, the fabrication of waveguides doped with gold nanoparticles with panoramic FOV and subsequent study of the total FOV enhancement would be another future work. Previous work of our group[34] has shown that waveguide encoded lattices (WELs) encoded 3D interconnected waveguides have panoramic FOV. Each WEL lattice consists a dense of identical pentadirectional waveguides, the five waveguide arrays oriented at different directions result in panoramic FOV and multiple corresponding imaging functionalities.[34]

a.

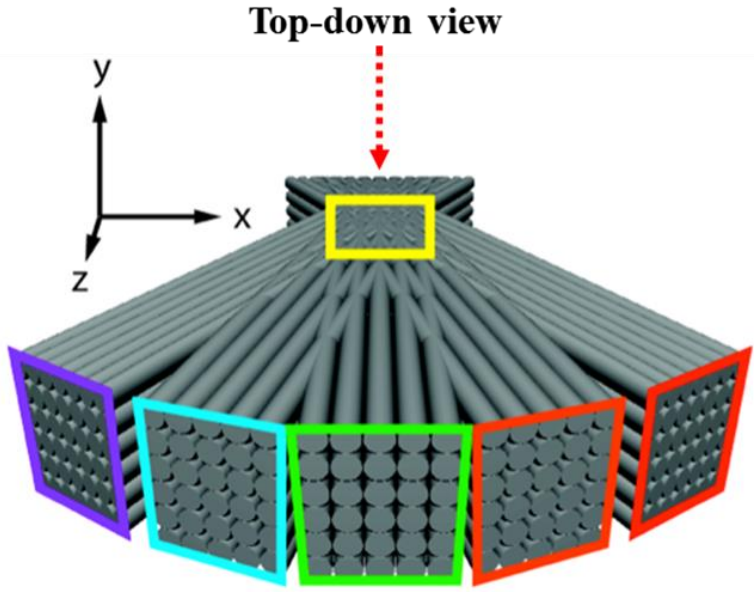

b.

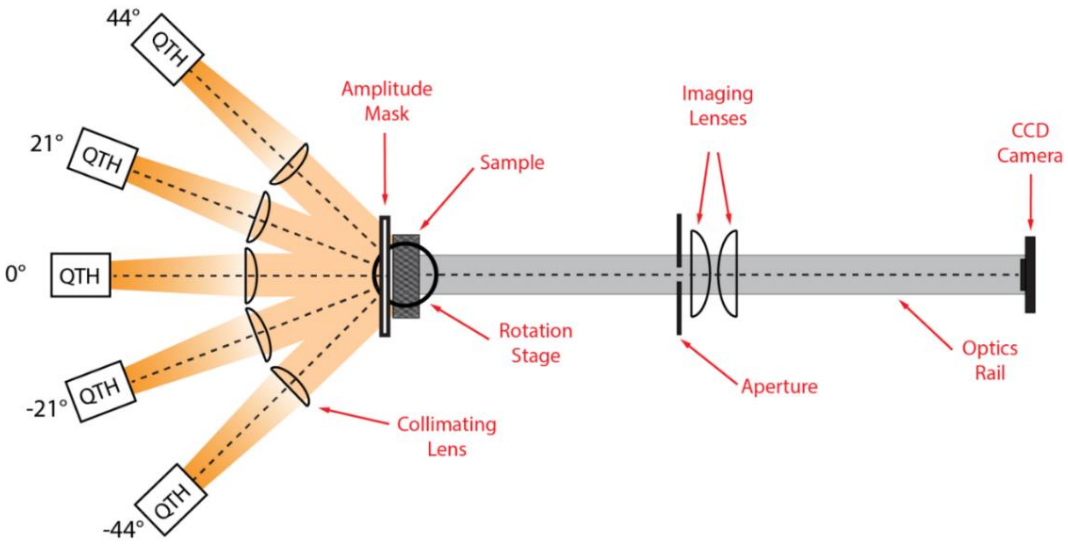

Figure 5.1 a) A scheme of the WEL, which shows the extension of each waveguide array along its axis and its corresponding relative angular position. Reprinted with permission from John Wiley and Sons [34]. Copyright © 2017 Wiley-VCH Verlag

GmbH & Co. KGaA, Weinheim. b) Scheme of optical assembly for the WELs fabrication. Reprinted with permission from [48].

For this thesis work, due to the significant enhancement of FOV for the 0° waveguide array doped with gold nanoparticles, we assume that WELs doped with gold nanoparticles also confer a substantial enhancement in the panoramic FOV. Thus, it's valuable to further fabricate WELs doped with gold nanoparticle and subsequently investigate its optical properties based on the panoramic FOV measurement.

External quantum efficiency (EQE) measurements for the gold doped waveguide and the undoped sample can be another branch for future work. EQE is the ratio of charge carriers extracted by the solar cell to incident photons.[49] Based on the results of my thesis work, the waveguide doped with gold nanoparticles has larger FOV than the undoped waveguide, so the gold nanoparticles doped waveguide structure are supposed to be able to capture wide-angle light. As the angle of light incident increases, according to Fresnel law, light transmitted into the solar cell decreases. However, since the gold nanoparticles doped waveguide film has larger acceptance range, EQE of the solar cell coated with the gold doped film is supposed to decrease slower. Therefore, it's also valuable to measure EQE for the waveguide doped with gold nanoparticles and the undoped sample.

Demonstration of metal nanoparticle doped polymer waveguides can lead to variety of new works. Since silver (i.e. Ag) as a noble metal nanoparticle also has numerous

physical and chemical properties, it has great potential in enhancing optical properties of the silver nanoparticles doped polymer waveguides. For this new research idea, we can start with the fabrication of silver nanoparticles doped epoxide waveguides and sequent study its optical properties. Yagci et al. have motioned the high possibility to fabricate silver-epoxy nanocomposite using photoinduced electron transfer and simultaneous cationic polymerization as a novel route.[42] Their approach is similar as the *in situ* method for preparing gold-acrylic nanocomposites through the free radical polymerization[42] which is easier than the preparation of gold-epoxy nanocomposites. For the future work of this thesis, it's interesting to modify the synthesis approach to go along with our white light self-trapping method, since the corresponding silver nanoparticles doped waveguide structures probably have several unique optical properties. The optical characterization may use same idea as this thesis work, it's valuable to measure FOV of the 0º metallodieletric waveguides and tune the change of FOV through modifying the fabrication conditions. As well, it's also interesting to attempt to study other potential optical properties of the silver nanoparticles doped epoxide waveguides.

References

1. M. A. Noginov, G. Zhu, A. M. Belgrave, R. Bakker, V. M. Shalaev, E. E. Narimanov, S. Stout, E. Herz, T. Suteewong and U. Wiesner, *Nature*, **2009**, *460*, 1110-1112.

2. M. W. Knight, H. Sobhani, P. Nordlander and N. J. Halas, *Science*, **2011**, *332*, 702-704.

3. S. Khatua, W. S. Chang, P. Swanglap, J. Olson and S. Link, *Nano Lett*., **2011**, *11*, 3797-3802.

4. B. Sepúlveda, P. C. Angelomé, L. M. Lechuga and L. M. Liz-Marzán, *Nano Today*, **2009**, *4(3)*, 244-251.

5. K. M. Mayer, J. H. Hafner and A. À. Antigen, *Chem*. *Rev*., **2011**, *111*, 3828–3857.

6. N. Liu, M. L. Tang, M. Hentschel, H. Giessen and a P. Alivisatos, *Nat*. *Mater*., **2011**, *10*, 631-636.

7. B. Park, S. H. Yun and etc, *Light Sci. Appl.*, **2014**, *3*, e222.

8. G. Carotenuto, B. Martorana, P. B. Perlo, L. J. Nicolais, *Mater. Chem.*, **2003**, *13*, 2927-2930.

9. M. Cavendish, Senses. Insect eyes, *Insects and Spiders of the World*, **2003**, *8*, 459. ISBN 0761473424.

10. R. Völkel, M. Eisner, K.J. Weible, Miniaturized imaging systems, *Microelectronic Engineering*, **2013**, *67-68*, 461-472.

11. K-H Jeong, J. Kim and L. P. Lee, *Science*, **2006**, *312*, 557-561.

12. D. Floreano, R. Pericet-Camara, S. Viollet, et al., Miniature Curved Artificial Compound Eyes, *Proc. Natl. Acad. Sci. U S A*, **2013**, *110 (23)*, 9267-9272.

13. P. Baker, C. Fermuller, and Y. Aloimonos, A Spherical Eye from Multiple Cameras (or How to Make Better Models). *Proceedings of Conference on Computer Vision and Pattern Recognition*, **2001**, *1*, 576-583.

14. G. Stegeman, M. Segev, *Science*, **1999**,*286*, 1518-1523.

15. A. Hudson, PhD Thesis, **2010**, McMaster University.

16. S. Trillo, W. Torruellas, *Spatial Solitons*, **2011**.

17. M. Mitchell, M. Segev, T.H. Coskllη, D.N. Christodolliides, *Phys. Rev. Lett.*, **1997**, *79*,4990- 4993.

18. A.W. Snyder, D.J. Mitchell, *Phys. Rev. Lett.*, **1998**, *80*, 1422-1424.

19. D. Christodolliides, T. H. Coshln, M. Mitchell, Z. Chen, M. Segev, *Phys. Rev. Lett.*, **1998**, *80*, 5113-5116.

20. D. Kip, M. Soljacic, M. Segev, E. Eugenieva, *Science*, **2000**, *290*, 495-498.

21. M. Mitchell, Z. Chen; M. Shih, M. Segev, *Phys. Rev. Lett.*, **1996**, *77 (3)*, 490-493.

22. M. Mitchell and M. Segev, *Nature*, **1997**, *387*, 880-883.

23. H. BlIljan, A. Siber; M. Soljacic, M. Segev, *Phys. Rev.*, **2002**, *66*.

24. S. Shoji, S. Kawata, *Appl. Phys. Lett.*, **1999**, *75*, 737.

25. A. Kewitsch, A. Yariv, *Opt. Lett.*, **1996**, *21*, 24-26.

26. A. Kewitsch, A. Yariv, *Appl. Phys. Lett.*, **1996**, *68*, 455-457.

27. I. B. Burgess, W. E. Shimmell, K. J. Saravanamuttu, Spontaneous Pattern Formation Due to Modulation Instability of Incoherent White Light in a Photopolymerizable Medium, *J. Am. Chem. Soc*. **2007**, *129*, 4738-4746.

28. J. Zhang, K. Kasala, A. Rewari, K. Saravanamuttu, Self-Trapping of Spatially and Temporally Incoherent White Light in a Photochemical Medium, *J. Am. Chem. Soc.* **2006**, *128*, 406-407.

29. K. Kasala and K. Saravanamuttu, Interactions of mutually incoherent self-trapped beams of white light in a photopolymerisable medium, *Appl. Phys. Lett.*, **2008**, *93*, 051111-051113.

30. J. Zhang and K. Saravanamuttu, The Dynamics of Self-Trapped Beams of Incoherent White Light in a Free-Radical Photopolymerizable Medium, *J. Am. Chem. Soc.*, **2006**, *128*, 14913-14923.

31. W.S. Shimmell, Master's Thesis, **2009**, McMaster University.

32. A.W. Snyder, and John D. Love, Optical Waveguide Theory, *New York: Chapman and Hall*, **1983**.

33. H. Lin, I.D. Hosein, K. Benincasa, and K. Saravanamuttu, Slim Films with Seamless Panoramic Fields of View: The Radially Distributed Waveguide Encoded Lattice (RDWEL), *Advanced Optical Materials*, **2018** (in revision).

34. I.D. Hosein, H. Lin, M.R. Ponte, et al., Waveguide Encoded Lattices (WELs): Slim Polymer Films with Panoramic Fields of View (FOV) and Multiple Imaging Functionality, *Adv. Funct. Mat.*, **2017**.

35. T. Pradeep, Noble Metal Nanoparticles, *Springer Handbook of Nanomaterials*, **2013**.

36. U. Kreibig and M. Vollmer, *J. Am. Chem. Soc.*, **1995**, *118*.

37. R. Karlsson, *J. Mol. Recognit.*, **2004**, *17*, 151-161.

38. C. J. Murphy, T. K. Sau, A. M. Gole, C. J. Orendorff, J. Gao, L. Gou, S. E. Hunyadi and T. Li, *J. Phys. Chem. B*, **2005**, *109*, 13857-13870.

39. P. Zhao, N. Li and D. Astruc, State of the art in gold nanoparticle synthesis, *Coord Chem Rev*, **2013**, *257*, 638-665.

40. J. Turkevich, P.C. Stevenson and J. Hillier, Nucleation and growth process in the synthesis of colloidal gold, *Discuss of the Faraday Society*, **1951**, *11*, 55-75.

41. Y. Yagci, M. Sangermano and G. Rizza, A visible light photochemical route to silver–epoxy nanocomposites by simultaneous polymerization–reduction approach, *Polymer*, **2008**, *49(24)*, 5195-5198.

42. Y. Yagci, M. Sangermano and G. Rizza, Synthesis and Characterization of Gold−Epoxy Nanocomposites by Visible Light Photoinduced Electron Transfer and Cationic Polymerization Processes, *Macromolecules*, **2008**, *41*, 7268-7270.

43. M. Sangermano, Y. Yagci and G. Rizza, In Situ Synthesis of Silver−Epoxy Nanocomposites by Photoinduced Electron Transfer and Cationic Polymerization Processes, *Macromolecules*, **2007**, *40*, 8827-8829.

44. Basker D. K., PhD Thesis, **2016**, McMaster University.

45. I. B. Burgess, M. Ponte, K. Saravanamuttu, Spontaneous formation of 3-D optical and structural lattices from two orthogonal and mutually incoherent beams of white light propagating in a photopolymerisable material, *J. Mater. Chem. C*, **2008**, *18*, 4133-4139.

46. K. Kasala, K. Saravanamuttu, Optochemical self-organisation of white light in a photopolymerisable gel: a single-step route to intersecting and interleaving 3-D optical and waveguide lattices, *J. Mater. Chem. C*, **2012**, *22*, 12281-12287.

47. M. R. Ponte, R. Welch and K. Saravanamuttu, An optochemically self-organized nonlinear waveguide lattice with primitive cubic symmetry, *Opt. Express*, **2013**, *4*, 4205-4214.

48. H. Lin, PhD Thesis, **2018**, McMaster University.

49. S.E. Shaheen, C.J. Brabec and et al., Sariciftci, 2.5% Efficient Organic Plastic Solar Cells, *Applied Physics Letters*, **2001**, *78(6)*, 841-843.

50. Y. Yagci, M. Sangermano, G. Rizza, *Chem. Commun*., **2008**, *24*, 2771–2773.

51. H. Li, Y. Qi, R. Malallah, and J.T. Sheridan, Modeling the Nonlinear Photoabsorptive Behavior during Self-Written Waveguide Formation in a Photopolymer, *J. Opt. Soc. Am. B*, **2015**, *32*, 912-922.

52. H. Li, Y. Dong, P. Xu, Y. Qi, C. Guo, J.T. Sheridan, Beam Self-Cleanup by Use of Self-Written Waveguide generated by Photopolymerization, *Opt. Lett.* **2015**, *40*, 2981-2984.

53. D. Floreano, et al., *Proc. Natl. Acad. Sci. U S A*, **2013**, *110(45)*, 9267-9171.

54. S. Shoji, S. Kawata, A.A. Sukhorukov, Y.S. Kivshar, *Opt. Lett.*, **2002**, *27*, 185.